Computational Analysis of Unidirectional Hybrid Composite Materials

Pedro de Herédia de Almeida

Thesis to obtain the Master of Science Degree in

Aerospace Engineering

Supervisors: Prof. José Arnaldo Pereira Leite Miranda Guedes
Prof. Hélder Carriço Rodrigues

Examination Committee

Chairperson: Prof. Filipe Szolnoky Ramos Pinto Cunha
Supervisor: Prof. Hélder Carriço Rodrigues
Member of the Committee: Prof. Aurélio Lima Araújo

November 2018

Acknowledgments

First, I would like to thank my supervisors Professor José Miranda Guedes and Professor Hélder Carriço Rodrigues of the Mechanical Engineering Department from Instituto Superior Técnico, University of Lisbon, for the guidance and support throughout the development of this master's thesis. Professor Miranda Guedes lent me his work, thus allowing me to develop my own, and has always shown readiness to update it according to my needs. Professor Carriço Rodrigues was the person that first introduced me to this research topic and provided the opportunity of writing this thesis. An additional thanks to Doctor António Melro for having generously provided his cross-sectional random fibre distribution algorithm `RAND_uSTRU_GEN`, which was his doctoral dissertation topic.

Secondly, I would like to express my deepest thanks to all my family and friends for their support at every moment of this journey. A special acknowledgement for all the support given by my parents, who provided the means for me to come this far, by my siblings, who always cheered me up, and by my girlfriend, who was always by my side and willing to help.

Finally, I would like to thank the school along with all the professors and colleagues with whom I have shared knowledge and tools that helped me complete my studies.

Resumo

O objectivo deste trabalho é desenvolver um modelo de elementos finitos para estudar o comportamento de compósitos unidireccionais, híbridos e não híbridos, quando sujeitos a cargas longitudinais. O estudo da hibridização visa o alcance da pseudo-ductilidade nos materiais compósitos.

De maneira a representar com mais precisão a microestrutura do material, é apresentado um novo método para obtenção da geometria da secção transversal de um volume elementar representativo com uma distribuição aleatória de fibras na matriz. O problema é abordado como um problema de optimização e resolvido com a ajuda de um algoritmo genético, e o método é capaz de atingir níveis elevados de fracção volúmica de fibras.

O estudo da homogeneização foi brevemente discutido e concluiu-se que para fibras arranjadas aleatoriamente há um ganho substancial nas propriedades do material quando comparado com uma disposição regular das fibras.

Finalmente, o modelo de dano da microestrutura foi implementado impondo extensões na direcção longitudinal das fibras. A falha das fibras é gradual para obter uma curva de tensão-extensão mais detalhada. São estudados resultados para dois compósitos reforçados por fibras de carbono distintas e a hibridização resultante da sua combinação. Os resultados mostram que a distribuição da resistência à tracção das fibras prevalece sobre a geometria da microestrutura no que respeita a sua influência no comportamento mecânico do material. O compósito híbrido estudado demonstra tendência para atingir um comportamento pseudo-dúctil, mas este desenvolvimento menos drástico da falha da microestrutura causa uma clara redução na resistência do material.

Palavras-chave: Compósitos unidireccionais, Hibridização, Aleatoriedade na distribuição de fibras, Homogeneização, Pseudo-ductilidade

Abstract

The objective of this work is to develop a finite element model to study the behaviour of unidirectional composites, hybrid and non-hybrid, when subjected to longitudinal loads. The study of the hybridization aims the achievement of pseudo-ductility in composite materials.

In order to represent with more precision the material microstructure, a new method to obtain the geometry of the transverse section of a representative volume element with a random distribution of fibres in the matrix is presented. The problem is approached as an optimization problem and solved with the help of a genetic algorithm, and the method is able to achieve high levels of fibre volume fraction.

The study of homogenization is briefly discussed and it is concluded that for randomly arranged fibres there is a substantial gain on the material properties when compared to a regular fibre packing.

Finally, the damage model for the microstructure is implemented imposing strains in the longitudinal direction of the fibres. The fibre failure is gradual so that the stress-strain curve obtained is more detailed. Results are studied for two non-hybrid composites reinforced with distinct carbon fibres and the resulting hybridization of the two types of fibres. The results show that the influence of fibre tensile strength distribution in the mechanical behaviour of the material prevails over the influence of the microstructure geometry. The studied hybrid composite demonstrates tendency to achieve a pseudo-ductile behaviour, but this less drastic development of the failure of the microstructure causes a clear decrease in the material strength.

Keywords: Unidirectional composites, Hybridization, Randomness in fibre distribution, Homogenization, Pseudo-ductility

Contents

Acknowledgments . . . iii
Resumo . . . v
Abstract . . . vii
List of Tables . . . xi
List of Figures . . . xiii
Nomenclature . . . xv

1 Introduction **1**
1.1 Motivation . . . 3
1.2 Objectives . . . 4
1.3 Thesis Outline . . . 5

2 RVE Geometry Development **7**
2.1 Theoretical Overview . . . 7
2.1.1 Methodologies to generate transverse randomness of reinforcement . . . 7
2.1.2 Nature-inspired optimization . . . 9
2.2 Analytical Model . . . 10
2.3 Implementation using MATLAB® . . . 16
2.3.1 Optimization with MATLAB® function `ga` . . . 19
2.3.2 Optimization with function `cuckoo_search` . . . 21
2.3.3 Modification for hybrid composites . . . 22
2.4 Statistical characterisation . . . 22
2.4.1 Time . . . 23
2.4.2 Voronoi polygon areas and neighbouring distances . . . 24
2.4.3 Examples of generated RVE geometries . . . 25

3 RVE equivalent properties **29**
3.1 Homogenization theory . . . 29
3.2 Implementation using PREMAT . . . 30
3.2.1 Generating finite element mesh with Gmsh . . . 31
3.2.2 Exporting the mesh to PREMAT . . . 33
3.3 Examples . . . 38

3.3.1 Parametric studies . . . 38
3.3.2 Random fibre arrangements . . . 39

4 Damage Model **43**
4.1 Problem Description . . . 43
4.2 Numerical Model . . . 44

5 Results **49**
5.1 Mechanical properties . . . 49
5.2 Influence of fibre distribution . . . 50
5.3 Influence of tensile strength distribution . . . 52
5.4 Carbon-carbon hybridization . . . 54
5.5 Stress distribution . . . 57

6 Conclusions **61**
6.1 Achievements . . . 61
6.2 Future Work . . . 62

Bibliography **65**

A Flowcharts for `RAND_uSTRU_GEN` **69**

List of Tables

2.1 Average and standard deviations of time in seconds required to run each algorithm for single fibre radius configuration. 23
2.2 Average and standard deviations of time in seconds required to run each algorithm for two different fibre radius. 23
2.3 Coefficient of variation for Voronoi polygon areas and distances to neighbouring fibres. . . 25

3.1 Selection of mesh refinement parameters 35
3.2 Parametric study for mesh refinement parameter `lc` 39
3.3 Parametric study for RVE size parameter δ 39
3.4 Results with regular and random distributions 40

5.1 Mechanical properties for carbon fibres. 49
5.2 Initial failure strain and stress, maximum stress and ultimate failure strain for different fibre arrangements. 51
5.3 Initial failure strain and stress, maximum stress and ultimate failure strain for different AS4 fibre strength distributions. 52
5.4 Initial failure strain and stress, maximum stress and ultimate failure strain for different M50S fibre strength distributions. 53
5.5 Initial failure strain and stress, maximum stress and ultimate failure strain for different AS4-M50S hybrid fibre strength distributions. 55

List of Figures

1.1 Schematic stress-strain diagrams for (a) non-hybrid composites, (b) typical hybrid composites, and (c) pseudo-ductile hybrid composites [19]. 4

2.1 Definition of RVE regions.[28] 8
2.2 Crossover operation with one-cut point. (a) Designs selected for crossover (parent chromosomes). (b) New designs (children) after crossover.[30] 9
2.3 Cuckoo Search.[31] 10
2.4 Separating the fibres. 11
2.5 Overlapping distance. 11
2.6 Coordinate system. 12
2.7 Geometric continuity: shaded areas count four full fibres. 13
2.8 Distances from first quadrant. 14
2.9 Remaining distances from second quadrant. 14
2.10 Remaining distances from third quadrant. 15
2.11 Flowchart for `randgenGA`. 17
2.12 Generating new circles to satisfy geometric periodicity. 18
2.13 Tuning Crossover Fraction. 21
2.14 Voronoi cells [28]. 24
2.15 Single fibre configuration: $V_f = 40\%$. 26
2.16 Single fibre configuration: $V_f = 50\%$. 27
2.17 Single fibre configuration: $V_f = 60\%$. 27
2.18 Fibre-hybrid configuration: $V_f = 40\%$. 27
2.19 Fibre-hybrid configuration: $V_f = 50\%$. 28
2.20 Fibre-hybrid configuration: $V_f = 60\%$. 28
2.21 Single fibre configuration: $V_f = 65\%$. 28

3.1 Periodic composite structure.[25] 30
3.2 Circular form in Gmsh. 32
3.3 Matrix loop (bold black line). 32
3.4 Node ordering for tetrahedra. 33
3.5 Node ordering for hexahedra. 34

3.6 Geometries generated in Gmsh for a fibre volume fraction of 60%. 35
3.7 Meshes obtained for RVE type 8. 36
3.8 Meshes obtained for RVE type 212. 37
3.9 Gmsh meshing error generating quads. 38
3.10 Analysed meshes for $V_f = 60\%$. 42
3.11 Meshing error situations. 42

4.1 Flowchart for the damage model. 45
4.2 Stress-strain behaviour for the damage model. 46

5.1 Analysed RVE geometries. 50
5.2 Stress-strain behaviour of AS4 composite for different fibre arrangements. 51
5.3 RVE FE meshes generated. 52
5.4 Stress-strain behaviour of AS4 composite for different tensile strength distributions. 53
5.5 Stress-strain behaviour of M50S composite for different tensile strength distributions. . . . 54
5.6 Hybrid configuration. 54
5.7 Stress-strain behaviour of hybrid AS4-M50S composite for different tensile strength distributions. 55
5.8 Stress-strain behaviour comparison for AS4 (blue) and M50S (yellow) non-hybrid composites and AS4-M50S (red) hybrid composite. 56
5.9 Element stress distributions for AS4 reinforced RVE. 57
5.10 Element stress distributions for M50S reinforced RVE. 57
5.11 Element stress distributions for AS4-M50S hybrid reinforced RVE. 59

A.1 Flowchart of algorithm `RAND_uSTRU_GEN` [28]. 69
A.2 Flowchart of STEP ONE [28]. 70
A.3 Flowchart of STEP TWO [28]. 71
A.4 Flowchart of STEP THREE [28]. 72

Nomenclature

Acronyms

2D	Two-dimensional.
3D	Three-dimensional.
CAD	Computer Aided Design.
CS	Cuckoo Search.
FBM	Fibre Bundle Model.
FE	Finite Element.
FEA	Finite Element Analysis.
FEM	Finite Element Method.
GA	Genetic Algorithm.
GLS	Global Load Sharing.
HE	High Elongation.
LE	Low Elongation.
LLS	Local Load Sharing.
PBC	Periodic Boundary Conditions.
RVE	Representative Volume Element.
SCF	Stress Concentration Factor.
SEM	Spring Element Model.
STDV	Standard Deviation.
UD	Unidirectional.

Greek symbols

χ	Solution for local deformation problems.

$\Delta\varepsilon$ Strain increment.

Δ_{min} Minimum distance parameter.

μ Average.

ν Poisson's ratio.

Ω Solid body.

ρ Coefficient of variance.

σ Standard deviation. Stress.

σ_0 Weibull scale parameter.

σ_T Tensile strength.

ε Micro-scale parameter. Strain.

Roman symbols

A Area.

a, b RVE dimensions.

D Homogenized elastic constants matrix.

d Distance.

E Young Modulus.

F Objective function.

f Overlapping distance.

G Shear Modulus.

g General function.

`ian` Mesh refinement parameter, PREMAT.

L Gauge length.

L_0 Characteristic gauge length.

`lc` Mesh refinement parameter, Gmsh.

m Weibull modulus.

n Number of subscript.

N_p Population size.

p Output matrix of `randgenGA`.

R Fibre radius.

r Rank of an individual in GA.

u Solution for deformation problems.

V Volume.

V_f Fibre volume fraction.

X Modes of deformation.

$\mathbf{x}$ Design variables vector.

x, y, z Cartesian components.

Subscripts

b Refers to broken.

e Refers to elements.

f Refers to fibres.

i, j, k, l Numerical indexes.

m Refers to matrix.

Y Refers to boundary.

Superscripts

ε Refers to micro-scale parameter.

f Refers to fibres.

k, l Numerical indexes.

Chapter 1

Introduction

Composite materials are becoming more and more important in industry. Their high performance in terms of stiffness and strength-to-weight ratio allows lighter yet stronger, more efficient structures, and so, nowadays fibre reinforced composites are considered the materials of the future, with applications in sporting goods (rackets, golf shafts, etc.), boats, civil construction, automotive and aerospace industry, and defense applications involving aircraft, rocket nozzles and nose cones of missiles and the space shuttle [1]. In the aerospace industry, the ultimate goal is to provide more economical and greener air transport by cutting fuel consumption and associated carbon dioxide emissions, which is mainly obtained by weight reduction, making it clear why the use of composites is essential and increasing in aircraft structures and engines [2].

Fibre reinforced composites are known as hierarchical materials with three structural levels: micro-scale, meso-scale and macro-scale. The micro-scale defines the arrangement of fibres in the fibre bundle, the intermediate level (meso-scale) generally relates to the fabric/lamina geometry, and the macro-scale refers to the engineering structural response of the material. In the framework of a multi-scale simulation of composite materials, micro-scale approaches (including both analytical methods and numerical methods) are usually applied to predict the effective stiffness and strength properties of transversely isotropic constitutive properties of composites, serving as theoretical tools for engineering structure design [3].

To model numerically an heterogeneous material mechanical behaviour from a micro-scale approach one can mesh the complete part and all of its constituents or consider the existence of a sufficiently small but representative volume element of the material to be analysed. It is clear that the first option would require very high computational efforts on meshing and analysis, but the second has been the subject of thorough studies as it provides a method to quantitatively characterize the material's mechanical behaviour without demanding an exaggerated computational effort. For this matter, the introduction of the representative volume element (RVE) was made by Hill [4]. For the author, the RVE must be structurally representative of the mixture of constituents on average, and contain a sufficient number of

inclusions for the apparent overall moduli to be effectively independent of the surface values of traction and displacement, as long as these are 'macroscopically uniform'.

In spite of the fact composites are generally composed by layers with different orientations, ultimate failure of composite structures is often dominated by failure of the load–aligned plies; this makes it particularly important to develop predictive models for the response of unidirectional (UD) composites under longitudinal tension [5].

The failure of UD composite materials is a complex process controlled by fibre breaks. One of the problems is that fibre tensile strength is a non-deterministic value. Since fibrous materials have a large surface area per unit volume, they are more likely to have surface defects than bulk materials. The presence of defects at random locations can lead to scatter in the experimentally determined strength values of fibres, which calls for a statistical treatment of fibre strength [1]. Thereby, it is important to find a statistical distribution to accurately represent the stochasticity of fibre strength. The Weibull distribution [6] is the most used with this objective, but others have proposed some changes and created modified versions. Peterlik and Loidl [7] found that the fibre strength is governed by more than one flaw population and therefore a bimodal Weibull distribution should be used. The Weibull of Weibulls (WOW) was created by Curtin [8] in an attempt to fix the problem of overestimation of the fibre strength at short gauge lengths when the traditional Weibull is utilized [9]. However, there is still no consensus whether traditional Weibull or the modified Weibull distributions better represent the fibre strength.

Fibre bundle models (FBM) are studied with the objective of understanding and anticipating the failure of UD composites [10]. The stochastic assignment of tensile strength means that some fibres have a relatively low strength. As the applied strain increases, these weakest fibres will fail first and locally lose their load-carrying ability. Consequently, the matrix carries stress away from the fracture point and the stress is redistributed among the intact fibres, leading to stress concentrations and increasing the probability of failure in nearby fibres. This causes a tendency to create clusters of broken fibres, which will grow and propagate unstably leading to the entire composite failure [11]. The stress redistribution can be predicted by global load sharing (GLS) models, which consider that the stress is redistributed uniformly among the intact fibres, not proving accurate when there is presence of matrix, or by local load sharing models (LLS), which depend on several parameters related to the geometry and the bounding between matrix and fibres. These last type of models introduce the definitions of stress concentration factor (SCF) and ineffective length. It is assumed that when a fibre breaks it locally looses the ability to carry stress, however, away from the failure plane it is still able to carry loads, which means that a fibre doesn't fully loose the ability to carry stress after it breaks. The SCF is an adimensional parameter that is defined as the ratio between the longitudinal stress in an intact fibre after the failure of a neighbour fibre and the longitudinal stress in the absence of breaks. The stress in the absence of breaks is usually considered the stress in the intact fibre far from the plane of break, which simplifies the determination of this parameter. The ineffective length is a measure of the stress recovery length of the fibre

and can be defined as twice the length at which the broken fibre can carry 90% of the applied stress [12].

Hybrid fibre-reinforced composites are defined as materials made by combining two or more different types of fibres in a common matrix, with the objective to offer a range of properties that cannot be obtained with a single kind of reinforcement [13]. The two fibre types are typically referred to as low elongation (LE) and high elongation (HE) fibres. The first fibre to fail is normally the LE fibre. The HE fibre does not necessarily have a large failure strain, but it is always larger than the one of the LE fibre [14]. Three types of configuration may be used for hybridization: interlayer, which consists in having different types of fibres in different layers, being that each layer only has a single fibre type; intralayer, where both types of fibres are stacked in a single layer; and intrayarn, also called fibre-by-fibre hybrids, consisting in having both fibre types in a single tow. This later type has proven to lead to better mechanical properties due to the greater dispersion of both fibre types [15].

1.1 Motivation

Modelling the random fibre distribution of a fibre-reinforced composite is of great importance when studying the progressive failure behaviour of the material on the micro-scale. Most of the existing methods regard the micro-scale geometry as a periodic structure, assuming a deterministic and ordered distribution of fibres. However, the realistic distribution of fibres has been known to be non-uniform and randomly distributed. Therefore, methods based on periodic fibre distributions cannot give accurate predictions of the effective properties of the composite. Random distributions instead of regular fibre packings lead to variations in fibre spacing resulting in significantly different stress distributions [16]. Wongsto and Li [17] compared the mechanical properties obtained for random and periodic distributions and concluded that the Young and shear moduli from UD composites have higher values for a random packing. Trias et al. [18] compared the strain and stress distributions for both types of arrangement and verified that the use of periodic models leads to underestimation of damage initiation.

The tensile failure of UD composites is a drastic process due to the propagation of clusters of broken fibres and hybridization can change this behaviour by changing the failure mechanisms in composite materials. Usually composite materials undergo catastrophic failure with a stress-strain diagram as presented in Figure 1.1(a). Hybridizing the composite material changes the failure process which results in stress-strain diagrams similar to Figure 1.1(b), where the two load drops correspond, respectively, to the failure of the LE fibres and the HE fibres. By understanding the controlling factors in the behaviour of hybrid composite materials it is possible to design a material with a pseudo-ductile behaviour, as illustrated in Figure 1.1(c).

A gradual failure of the composite allows its identification before the material looses its structural integrity. This way, it is possible to reduce enforced safety factors in the composite design. The first model to study the behaviour of hybrid composites was developed by Zweben [13] using an extended shear

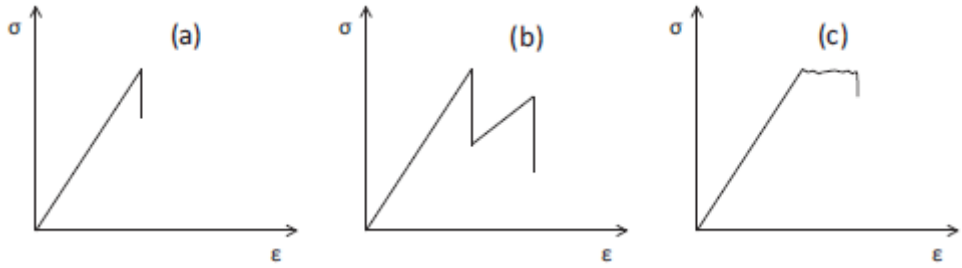

Figure 1.1: Schematic stress-strain diagrams for (a) non-hybrid composites, (b) typical hybrid composites, and (c) pseudo-ductile hybrid composites [19].

lag model for hybrid composites with an one-dimensional arrangement of alternating HE and LE fibres and considered the determination of the hybrid effect as a function of fibre properties.

More recently, a lot of effort is being made regarding the prediction of tensile failure of UD composites and their hybrid behaviour. Pimenta et al. [5] made use of a model applying cyclic longitudinal tension to predict the response of UD composites. Turon et al. [20] developed a progressive damage model based on fibre fragmentation, which was extended by Tavares [21] for the study of hybrid composites. In this later author master thesis, a dry tow model was also developed to predict the effects of fibre hybridization without matrix concerns, and additionally a micromechanical model taking into account the more complex mechanisms such as the damage in the matrix, fibres and interface. Conde et al. [22] used both the dry tow and the progressive damage model to optimize the material properties for the closest pseudo-ductile stress-strain curve. Tavares et al. [23] applied the spring element model (SEM) proposed by Okabe et al. [24] for random hybrid fibre packings. The model was created as an alternative to 3D FEM to provide low computational cost. The SEM is based on the assembly of periodic packages of fibre and matrix spring elements and takes into account local stress redistribution due to fibre failure. However, in spite of the computational effort 3D FEM provide more accuracy and can portray better the reality by providing continuous mesh surfaces and volumes connecting fibres and matrix.

1.2 Objectives

The objective of this work is to develop a three-dimensional micromechanical damage model to predict the tensile failure of UD composites and take into account the possibility of hybridization. The goal is to provide a tool that can study the composite behaviour when uniaxial traction is applied in the fibres longitudinal direction, both by obtaining the stress-strain curves and by observing the stress distribution. The main focus is to study what are the mechanical factors needed for the achievement of pseudo-ductility.

For that matter the use of a representative volume element with random distribution of fibres is essential and so a simple algorithm to obtain these kinds of geometries will be developed with the concern of permitting more than one fibre type/radius. The effect of the variation of fibre arrangements on the RVE equivalent properties will also be a research topic, with the help of the computational programs

developed by Guedes and Kikuchi [25] for the implementation of the homogenization theory and the calculation of stress distribution in the microstructure.

The comprehension of the fibrous materials behaviour considering the stochastic values for fibre tensile strength is also a challenge that will be addressed. This will influence the way the stress is redistributed after a fibre fails and it is important to understand the mechanisms of longitudinal fracture that might lead to clusters of broken fibres. Using the models presented above, this work results might serve to validate and test optimal solutions for pseudo-ductility provided by simpler models of composite behaviour prediction.

1.3 Thesis Outline

This thesis is organized by chapters that address different topics that are connected to the main goal of providing a micromechanical model for the understanding of the tensile failure of UD hybrid and non-hybrid composites.

Chapter 2 presents the design of the RVE geometry with a random fibre distribution. The problem of achieving random transverse sections of reinforcement is discussed and a new simple algorithm is developed using nature-inspired optimization. The algorithm is capable of achieving high fibre volume fractions and generate easily geometries for fibre hybrid composites. Statistical characterization is conducted to compare it with other methods.

In Chapter 3 the homogenization theory is applied to the generated RVE using PREMAT software. The finite element mesh is therefore created and the software's compatibility with an open-source three-dimensional mesh generator is studied. Parametric studies are conducted taking into account the mesh element size and the size of the microstructure. Another topic considered is the influence of regular fibre packings instead of random distributions on the computed equivalent material properties.

Combining the previous chapters the damage model to study the tensile failure of UD composites is presented in Chapter 4. The problem imposed by the model is described, including damage initiation and ultimate failure criteria, along with the numerical implementation to induce longitudinal loading. POSTMAT program is used for the finite element analysis in the stress and strain computations.

The results for carbon reinforced composites are found in Chapter 5. The influence of different geometries and of the stochastic values for the tensile strength of the fibres is analysed. The damage model is implemented for two non-hybrid composites and then the two different fibres are combined to form a carbon-carbon hybrid composite material. The stress-strain behaviours are presented for the analysed microstructures and the mechanical response is discussed with the aim of understanding the possibility of achieving pseudo-ductility.

Finally, Chapter 6 gives a summary of the achievements and a discussion of applications and possible future work in the mechanics of hybrid composites.

Chapter 2

RVE Geometry Development

In this chapter it will be presented the MATLAB® script developed for the generation of the RVE geometry of randomly distributed fibres using an optimization approach with a genetic algorithm (GA). The idea is to create a simpler and equally efficient model comparing to those already found in literature, by taking advantage of MATLAB® optimization toolbox.

2.1 Theoretical Overview

2.1.1 Methodologies to generate transverse randomness of reinforcement

There are several methodologies in the literature providing random point distributions for a given area, which can be applied in the representative volume element design.

The Poisson point pattern creates a random arrangement of points ensuring that the probability of finding a point in any coordinate of the area of interest is always the same. However, the created points cannot represent accurately the fibre distribution in a RVE, as they have no radius. Thus, an important role of this method is to serve as a comparative model to recognize aggregate or regular patterns.

Hard-core models define the points as the centres of each fibre, and imposes that the probability of finding a point at a distance to another point less or equal the fibre diameter is null, ensuring no overlapping between fibres. The problems with this approach are the high computational effort and the inability to reach fibre volume fractions greater than 55% [26].

Other method used to get an RVE geometry is through digital image analysis. The technique consists in acquiring several microscopic images of the material in study and join all these images in a mosaic. After that, with image processing a clear contrast between matrix and fibre can be established. Yang et al. [27] is an example of this method application. Although allowing a perfect replica of a sample of the transverse section of the material, this technique is extremely time and resource consuming.

By perturbing an hexagonally periodic pattern, Wongsto and Li's [17] algorithm can generate random fibre arrangements with high fibre volume fraction. It starts by choosing a direction to move the fibre from its position using a random angle from 0 to 2π. The maximum displacement the fibre can suffer is defined by the smallest of the distances to the border of the RVE and to the point where the fibre collapses with another one. By multiplying this maximum distance by a factor randomly generated between 0 and 1, the next position of the fibre is set. The process is repeated for all fibres at least 250 times, and stops when the required volume fraction is reached, leading to a very random geometry. However, there is the risk that the algorithm falls into a never ending loop, due to the randomness in generating the displacement direction.

Finally, Melro [28] developed a three-step procedure for generation of random fibre distribution, which includes a hard-core model (initial generation of fibres) and two heuristics, one consisting on stirring the fibres and the other affecting the fibres in the outskirts (regions 2-9 in Figure 2.1). The algorithm is able to quickly generate random distributions for high values of fibre volume fractions. The hard-core model starts by generating a fibre randomly located in the middle region of the RVE (region 1 in Figure 2.1). After that, a new fibre position is generated avoiding "collision" with the previous one. As the fibres are generated, the fibre volume fraction is updated. If the requested volume fraction cannot be reached, the algorithm moves to the second step, where the fibres are stirred towards each other creating matrix-rich areas. When all fibres are stirred, the algorithm moves to the third step where the fibres in the outskirts are moved away from the edges of the RVE. This also creates more space for further fibre placing and also prevents tangent circles in the area of interest boundaries. The algorithm flowcharts can be seen in Appendix A. This method's performance will be compared to the newly generated method. A modification to allow hybrid composites (two different fibre radius) will also be compared.

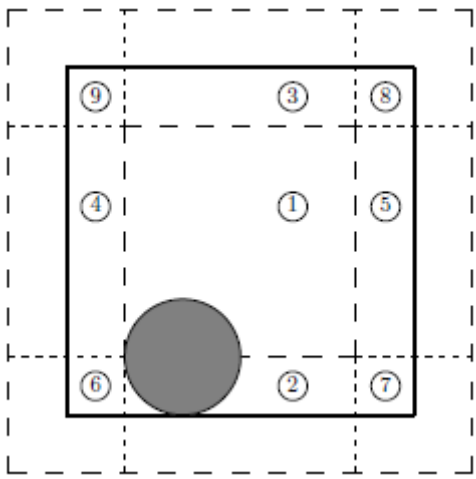

Figure 2.1: Definition of RVE regions.[28]

2.1.2 Nature-inspired optimization

As mentioned, a new model to generate transverse randomness of fibre reinforcements will be implemented using a genetic algorithm to minimize a proper measure of fibre distribution.

The choice of a metaheuristic (e.g. genetic) algorithm, is due to the objective function highly non-convex character, with the inherent existence of multiple local minima, and the lack of gradient information. Adding to that, they are easy to implement since they do not require continuity or differentiability of problem functions. The drawback is the large amount of function evaluations required for even reasonably sized problems [29].

Genetic algorithms are based on Darwin's theory of natural selection. The basic idea of the approach is to start with a set of designs, called the population, by randomly generating N_p genetic strings, or chromosomes, where N_p represents the population size. Each design is assigned a fitness value regarding the cost function. The objective of the GA is to generate a new set of designs from the current set such that the average fitness of the population is improved. The process is continued until a stopping criterion is satisfied or the number of iterations exceeds a specified limit. Three genetic operators are used to accomplish this task: reproduction, crossover, and mutation [30].

Reproduction is an operator where an old design is copied into the new population according to the design's fitness. There are many different strategies to implement this reproduction operator. This is also called the selection process.

Crossover corresponds to allowing two selected members of the new population to exchange characteristics of their designs among themselves. Crossover requires selection of starting and ending positions on a pair of randomly selected strings (called mating strings), and simply exchanging the string of 0's and 1's between these positions. Figure 2.2 illustrates this process.

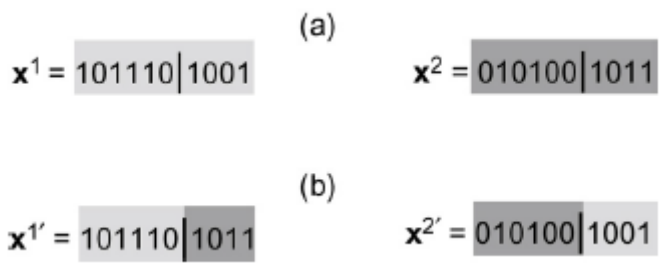

Figure 2.2: Crossover operation with one-cut point. (a) Designs selected for crossover (parent chromosomes). (b) New designs (children) after crossover.[30]

Mutation is the third step that safeguards the process from a complete premature loss of valuable genetic material during reproduction and crossover. In terms of a binary string, this step corresponds to

selection of a few members of the population, determining a location on the strings at random, and switching 0 to 1 or vice versa.

Since more fit members of the population are used to create new designs, the successive sets of designs have a higher probability of having members with better fitness values.

Another nature-inspired optimization algorithm was found in the literature and can be of use in this type of discipline: the Cuckoo search algorithm [31].

This method is based on cuckoo breeding behaviour, which is curious as they use another birds nests to lay their eggs. The choice of the nest is almost completely random but some cuckoos have evolved to mimic other birds in order to avoid being found. The search walk is generated with the use of Lévy flights, which was shown to be similar to the flight behaviour of some animals and insects [32].

The cuckoo search algorithm follows the procedures in Figure 2.3.

```
Objective function f(x),  x = (x_1, ..., x_d)^T;
Initial a population of n host nests x_i (i = 1, 2, ..., n);
while (t <MaxGeneration) or (stop criterion);
  Get a cuckoo (say i) randomly by Lévy flights;
  Evaluate its quality/fitness F_i;
  Choose a nest among n (say j) randomly;
  if  (F_i > F_j),
      Replace j by the new solution;
  end
  Abandon a fraction (p_a) of worse nests
      [and build new ones at new locations via Lévy flights];
  Keep the best solutions (or nests with quality solutions);
  Rank the solutions and find the current best;
end while
Postprocess results and visualisation;
```

Figure 2.3: Cuckoo Search.[31]

It can be seen that the selection of the best by keeping the best nests or solutions is equivalent to some form of elitism commonly used in the genetic algorithm, which ensures the best solutions are passed onto the next iteration.

2.2 Analytical Model

Since an optimization approach is considered, the first step is the problem formulation.

The objective is to find a random fibre distribution for a given fibre volume fraction in a fixed size repre-

sentative volume element, where the fibres do not touch each other, as that would lead to impossible designs. Suppose that we start with a random distribution of circles in a bounded area. It will be expected that some circles overlap each other. The goal is, starting with this random arrangement, to separate the circles whit overlap, as illustrated in Figure 2.4.

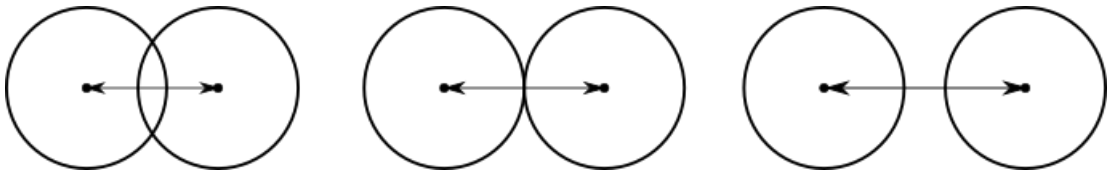

Figure 2.4: Separating the fibres.

To achieve this goal a proper measure (objective function) must be defined for minimization. Notice that stating that the fibres cannot touch each other means that the overlapping distance must be null. Looking at Figure 2.5 the overlapping distance f between two fibres with radius R_1 and R_2 can be defined by the simple formula:

$$f = R_1 + R_2 - d \tag{2.1}$$

where d represents the distance between both fibres. Studying the formula, one can conclude that:

- $f > 0$ if the circles overlap each other;
- $f = 0$ if the circles are tangent;
- $f < 0$ if the circles are separated.

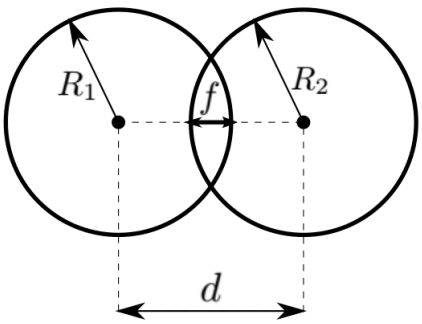

Figure 2.5: Overlapping distance.

This means that, in order to achieve a possible design, f must be at least null, as it was previously mentioned. Nevertheless, if minimization is conducted, a negative value leads to the best solution. However, more than two fibres exist in the RVE, so the condition required is that $f \leq 0$ for all possible pairs of fibres, or that the sum of all overlapping distances is at least null. We have found our optimization objective function:

$$F(\mathbf{x}) = \sum f \tag{2.2}$$

Now it is important to define the design variables $\mathbf{x}$. Consider a rectangular RVE with fixed dimensions $a \times b$, where the fibre centre positions are given by the coordinate system based in the bottom left corner of the RVE (Figure 2.6).

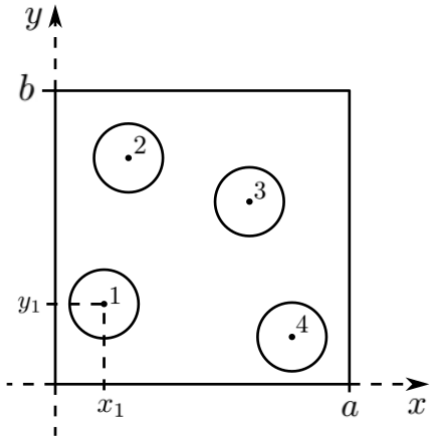

Figure 2.6: Coordinate system.

From (2.1) we can see that the objective function depends on the fibre radius and the distance between the fibres, which is calculated from their centre point positions. For any two fibres i and j, $i \neq j$:

$$d_{ij} = \sqrt{(x_i - x_j)^2 + (y_i - y_j)^2} \tag{2.3}$$

represents the distance between them. Since the fibre radius will be considered as a known constant parameter, the only variables are the centre point coordinates.

To completely define the design variables the next step is to find how many points, i.e. how many fibres will be inside the RVE. Since a later use of the RVE geometry will require periodic boundary conditions on the RVE, geometrical continuity between opposite sides of the generated distribution must be imposed. This means that even if the fibres are cut by the limits of the RVE, the fibre will still be completely inside the RVE with the contribution of the opposite side (Figure 2.7). Hence, the number of fibres inside the RVE will always be an integer number, that can be a priori calculated, and will now be explained.

The parameters already stated are the dimensions a, b of the RVE and the radius R of the fibres[1]. As we are dealing with composite materials, the remaining parameter is the fibre volume fraction required V_f. In UD composites, the fibre volume fraction can be assumed as a fibre area fraction when we look at the transverse section. This means that the fibre volume fraction can be calculated by:

$$V_f = \frac{A_f}{A_f + A_m} \tag{2.4}$$

[1] for a matter of simplicity, for now all fibres are considered to have the same radius

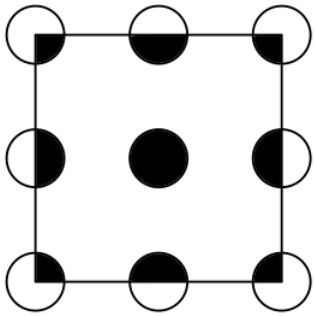

Figure 2.7: Geometric continuity: shaded areas count four full fibres.

where A_f and A_m represent the total area occupied by fibres and matrix on the RVE, respectively. Since the total area of the RVE is given by

$$A_{total} = A_f + A_m = a \times b \tag{2.5}$$

and the partial area occupied by the fibres is given by

$$A_f = n_{fibres} \times \pi \times R^2 \tag{2.6}$$

we can finally get the number of fibres necessary for the fibre volume fraction required:

$$n_{fibres} = \frac{V_f \times a \times b}{\pi \times R^2} \tag{2.7}$$

Since the number of fibres is an integer number, the result obtained from (2.7) should be substituted by the closest integer number. This implies that the real fibre volume fraction can be slightly different than the required one, which is not a problem as long as the number of fibres is sufficiently large.

The design variables vector (coordinates of each fibre centroid) can now be set:

$$\mathbf{x} = (x_1, ..., x_{n_{fibres}}, y_1, ..., y_{n_{fibres}}) \tag{2.8}$$

where, of course, $0 \leq x_i \leq a,\ 0 \leq y_i \leq b$ for $i = 1, ..., n_{fibres}$.

To analyse the objective function dependency on the design variables, we go back to Equation (2.3) where the distance is calculated based on these variables. Since we are dealing with a 2D RVE, that will repeat itself in both coordinate directions (periodicity), we have to account for the distances between each fibre and all the neighbouring ones. Consider a RVE with four fibres as illustrated in Figure 2.8. Admit that $d_{ij} = d_{ji}$ represent the distance between the fibres i and j. If we suppose that fibre 1 is moved slightly to the left, the distance to fibre 2, d_{12}, can no longer be measured by the distance to the circle illustrated in the same square, but to the repetition of that circle contained in the square on its left side, with centroid coordinates $(x_2 - a, y_2)$. This means that the repetition permits different manners

to calculate the distance between each pair of fibres, but we must only take into account the one that returns the smallest distance, i.e. the distance cannot be directly calculated from Equation (2.3), but it must consider the different hypothesis given by the repetition of the RVE. Figures 2.8 to 2.10 illustrate the different hypothesis to measure the distance from each fibre. Looking at Figure 2.8 we can see that there are two possibilities to measure d_{12} (dashed lines), two possibilities to measure d_{13} (dotted lines) and four possibilities to measure d_{14} (solid lines). From Figure 2.9 we find two ways of measuring d_{23} (dashed lines) and four ways of measuring d_{24} (solid lines), remaining the measurement of d_{34} that has also two possibilities as seen in Figure 2.10.

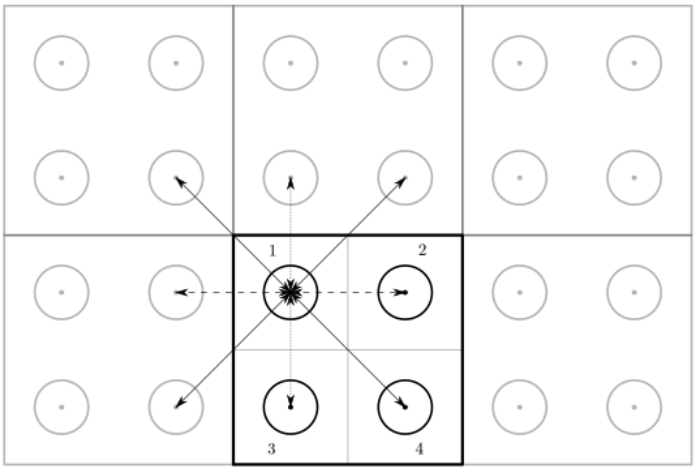

Figure 2.8: Distances from first quadrant.

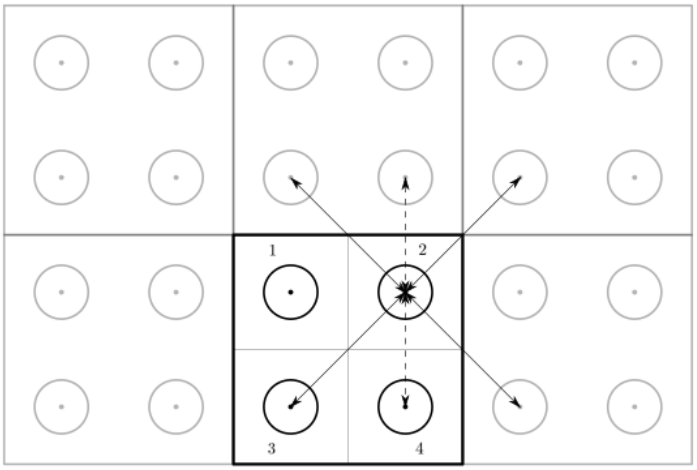

Figure 2.9: Remaining distances from second quadrant.

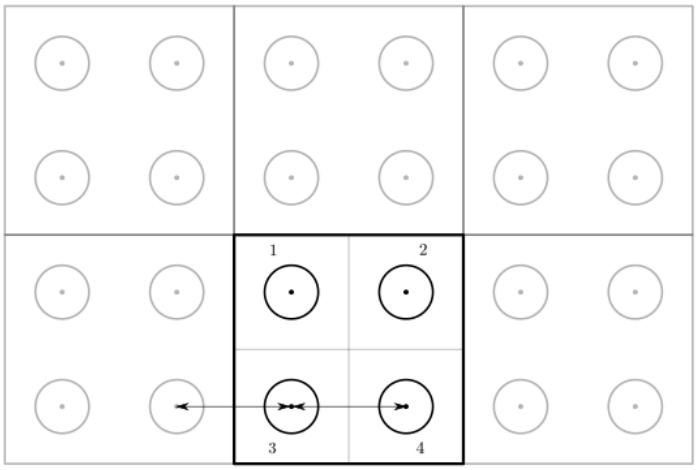

Figure 2.10: Remaining distances from third quadrant.

Therefore, the equations for the distances $d_{ij} = d_{ji}$ are:

$$d_{12} = min \begin{pmatrix} \sqrt{(x_1 - x_2)^2 + (y_1 - y_2)^2} \\ \sqrt{(x_1 - (x_2 - a))^2 + (y_1 - y_2)^2} \end{pmatrix} \tag{2.9}$$

$$d_{13} = min \begin{pmatrix} \sqrt{(x_1 - x_3)^2 + (y_1 - y_3)^2} \\ \sqrt{(x_1 - x_3)^2 + (y_1 - (y_3 + b))^2} \end{pmatrix} \tag{2.10}$$

$$d_{14} = min \begin{pmatrix} \sqrt{(x_1 - x_4)^2 + (y_1 - y_4)^2} \\ \sqrt{(x_1 - (x_4 - a))^2 + (y_1 - y_4)^2} \\ \sqrt{(x_1 - x_4)^2 + (y_1 - (y_4 + b))^2} \\ \sqrt{(x_1 - (x_4 - a))^2 + (y_1 - (y_4 + b))^2} \end{pmatrix} \tag{2.11}$$

$$d_{23} = min \begin{pmatrix} \sqrt{(x_2 - x_3)^2 + (y_2 - y_3)^2} \\ \sqrt{(x_2 - (x_3 + a))^2 + (y_2 - y_3)^2} \\ \sqrt{(x_2 - x_3)^2 + (y_2 - (y_3 + b))^2} \\ \sqrt{(x_2 - (x_3 + a))^2 + (y_2 - (y_3 + b))^2} \end{pmatrix} \tag{2.12}$$

$$d_{24} = min \begin{pmatrix} \sqrt{(x_2 - x_4)^2 + (y_2 - y_4)^2} \\ \sqrt{(x_2 - x_4)^2 + (y_2 - (y_4 + b))^2} \end{pmatrix} \tag{2.13}$$

$$d_{34} = min \begin{pmatrix} \sqrt{(x_3 - x_4)^2 + (y_3 - y_4)^2} \\ \sqrt{(x_3 - (x_4 - a))^2 + (y_3 - y_4)^2} \end{pmatrix} \tag{2.14}$$

It is clear that the distance will not only depend on the coordinates x_i, y_i of the fibre centres but also on the dimensions a and b of the RVE, as well as the objective function, which also depends on the fibre radius R. Note that each fibre represents any fibre with centre located at the same "quadrant" as the ones illustrated, i.e. fibre 1 represents the fibres with centroid coordinates $(x, y) \in ([0, a/2],]b/2, b])$, fibre 2 represents the fibres with centroid coordinates $(x, y) \in (]a/2, a],]b/2, b])$, fibre 3 represents the fibres with centroid coordinates $(x, y) \in (]a/2, a], [0, b/2])$ and fibre 4 represents the fibres with centroid coordinates $(x, y) \in ([0, a/2], [0, b/2])$.

The optimal design problem can finally be stated:

$$\begin{aligned} \text{minimize} \quad & F(\mathbf{x}, R, a, b) \\ \text{w.r.t.} \quad & \mathbf{x} = (x_1, ..., x_{n_{fibres}}, y_1, ..., y_{n_{fibres}}) \\ \text{subject to} \quad & 0 \leq x_i \leq a,\ 0 \leq y_i \leq b, \text{ for } i = 1, ..., n_{fibres} \end{aligned} \tag{2.15}$$

The genetic algorithm used for this purpose must reach a stopping criterion. Going back to Equation (2.1), we stated that the overlapping distance f calculated is capable of assuming negative values, thus causing the possibility of the objective function to have negative values as well. This can compromise the GA performance since the minimum reachable value of the function is uncertain, making it impossible to set a stopping criterion regarding this quantity. In order to set a minimum for the objective function, we must thwart the possibility of negative values by introducing a suitable adaptation for the overlapping distance f:

- $f > 0$ if the circles overlap each other;
- $f = 0$ if the circles do not overlap (if they are tangent or separated).

This can be accomplished replacing Equation (2.1) by

$$f = \begin{cases} 2R - d, & \text{if } d < 2R. \\ 0, & \text{otherwise.} \end{cases} \tag{2.16}$$

Thus for the objective function $F = \sum f$ will only contribute the fibres that are truly overlapping. If no overlapping is found, we get the minimum function value min$(F) = 0$.

2.3 Implementation using MATLAB®

Based on the model explained in 2.2 a MATLAB® script named `randgenGA` was created. The flowchart of the model is presented in Figure 2.11. It can be seen that the model is very simple and straightforward.

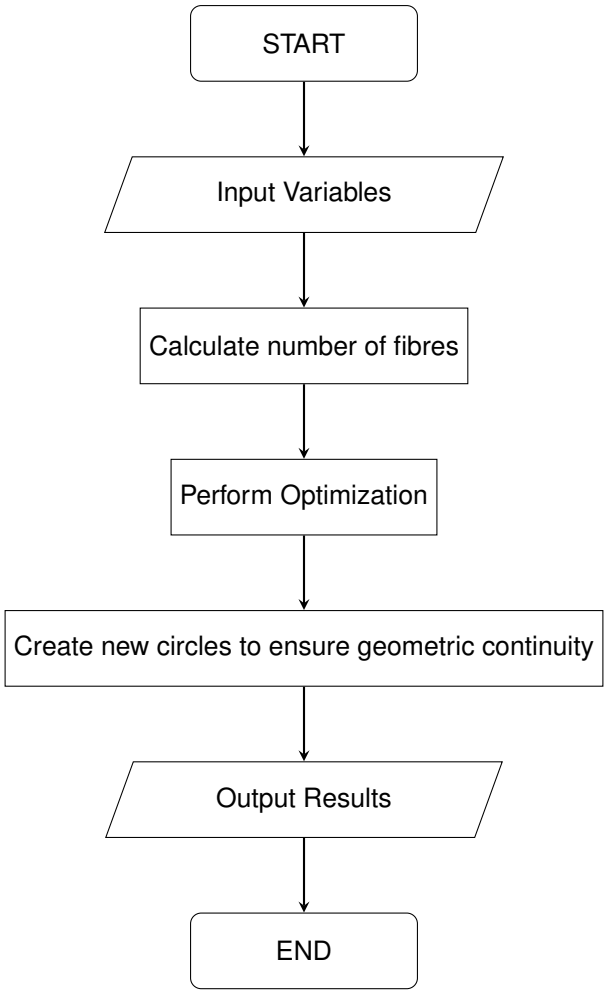

Figure 2.11: Flowchart for `randgenGA`.

For future comparisons with other methods, a square RVE will be assumed with side length given by:

$$a = b = \delta \times R \tag{2.17}$$

replacing a and b parameters by a ratio δ. These parameters can still be modified if the form of the RVE is not a square.

Due to the necessity of using this geometry in future finite element analysis, an additional parameter is needed. Since the objective function minimum value of 0 may be reached with touching fibres, a minimum distance must be imposed so that there is enough space to have a finite element representing the matrix material between the fibres. This minimum distance will be set equal to a percentage (Δ_{min}) of the radius R which will be added it to Equation (2.16).

Summing up, the input variables include:

- `R` - Fibre radius R.
- `delta` - Ratio δ defining the size of the RVE.

- `Vol_fibre` - Fibre volume fraction V_f required by the user.
- `mindist` - Percentage Δ_{min} defining the minimum distance allowed between neighbour fibres.

Then, since the size of the design variables vector is given by the number of fibres, we must use Equation (2.7) before entering the main step of optimization. For this step, the MATLAB® incorporated function `ga` performs the genetic algorithm. An alternative method is to use the cuckoo search algorithm with the MATLAB® script `cuckoo_search.m` provided by Yang and Deb [31] and for that purpose the script `randgenCS` was also written. The only difference between this alternative method and the main one is the optimization technique used. All variables, bounds and objective function remain the same, and so the flowchart on Figure 2.11 may also illustrate the process of `randgenCS`. The optimization procedures of both algorithms in MATLAB will be explained in Sections 2.3.1 and 2.3.2.

After the optimal design problem is solved and the fibre distribution is found, we must ensure that there is geometric continuity between opposite sides of the RVE so that periodic boundary conditions can be applied. This is achieved by generating n_{pbc} new circles based on the positions (x_i, y_i) of the ones that are crossing the boundaries and are not yet contributing as a full fibre. As stated before, the number of points generated is equal to the number of fibres found for the volume fraction requested. However, this means that the circles cutting the edges of the RVE were not yet copied to the opposite edge. If there are circles cutting the boundary lines they must be replicated in the opposite boundary (fibres 2 and 3 in Figure 2.12). Furthermore, if there is a circle in a RVE corner, then it should be replicated in the three remaining corners (fibre 4 in Figure 2.12).

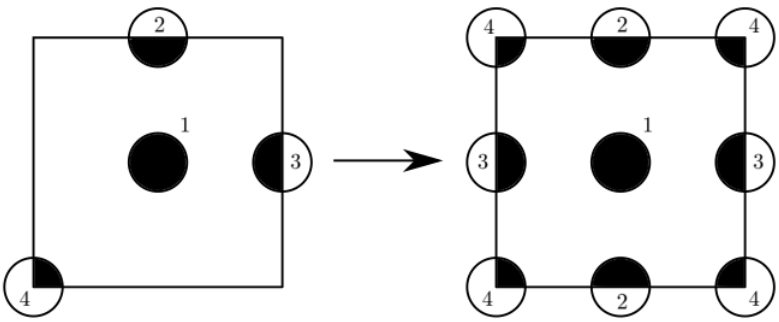

Figure 2.12: Generating new circles to satisfy geometric periodicity.

The model outputs a matrix $p_{m\times 4}$ where $m =$ total number of circles generated $(n_{fibres} + n_{pbc})$ and the four columns represent respectively:

- the coordinate x_i of the circle i centre point;
- the coordinate y_i of the circle i centre point;
- the radius R_i of the circle i [2];
- the number of the fibre correspondent to the circle (useful for the circles generated in the last step).

[2] in this case $R_i = R\ \forall i \in [1, n_{fibres}]$ but for further application of hybrid composites the radius will differ.

2.3.1 Optimization with MATLAB® function `ga`

The genetic algorithm call in MATLAB® is made using

```
x = ga(fun,nvars,A,b,Aeq,beq,lb,ub,nonlcon,options)
```

which finds a local minimum `x` for the objective function `fun`, with dimension (number of design variables) `nvars`, subject to linear constraints `Aeq*x=beq` and `A*x≤b` and nonlinear constraints defined by `nonlcon`, and defines a set of lower and upper bounds `lb` and `ub` on the design variables. The remaining input `options` controls the optimization parameters, replacing the default choices assumed by the software [33].

Looking to the optimization problem already formulated (2.15) there are neither linear nor non-linear constraints, so the inputs defining these constraints will not be used.

A function named `overlap` was written to evaluate the objective function `fun`. It computes the distances between the fibre centres based on Equations (2.9)-(2.14) and then calculates the overlapping distances according to (2.16) and sums them to get the value of the objective function F.

The number of design variables `nvars` is two times the number of fibres required, corresponding to the n_{fibres} values of x coordinates plus the n_{fibres} values of y coordinates (see (2.8)). The left bound `lb` is a vector with `nvars` null entries and the right bound is a vector where the first n_{fibres} values are equal to a and the remaining n_{fibres} values are equal to b, according to the condition $0 \leq x_i \leq a,\ 0 \leq y_i \leq b$ for $i = 1, ..., n_{fibres}$.

Finally, we need to define the state structure `options`. Several parameters are crucial to define the GA, as well as the functions used in the stochastic processes of reproduction, crossover and mutation. For the optimization of the function `overlap`, if not specified otherwise, the used functions and parameter values used were the MATLAB® default ones.

It is important to define the population size N_p. For that purpose, the parameter `PopulationSize` specifies how many individuals there are in each generation. With a large population size, the genetic algorithm searches the solution space more thoroughly, thereby reducing the chance that the algorithm returns a local minimum that is not a global minimum. However, a large population size also causes the algorithm to run more slowly. The default value for this parameter is `200`.

For the reproduction process, `ga` makes use of fitness scaling to convert the raw fitness scores that are returned by the fitness function to values in a range that is suitable for the selection function. The default fitness scaling function, `Rank`, scales the raw scores based on the rank of each individual instead of its score. The rank of an individual is its position in the sorted scores. An individual with rank r has

scaled score proportional to $1/\sqrt{r}$. So the scaled score of the most fit individual is proportional to 1, the scaled score of the next most fit is proportional to $1/\sqrt{2}$, and so on. Rank fitness scaling removes the effect of the spread of the raw scores. The square root makes poorly ranked individuals more nearly equal in score, compared to rank scoring.

With the fitness scaling done, there are many different strategies to implement the selection process. The `ga` default selection function, `Stochastic uniform`, lays out a line in which each parent corresponds to a section of the line of length proportional to its scaled value. The algorithm moves along the line in steps of equal size. At each step, the algorithm allocates a parent from the section it lands on. The first step is a uniform random number less than the step size [34].

Next, other genetic parameters specify how the genetic algorithm creates children for the next generation:
`EliteCount` specifies the number of individuals that are guaranteed to survive to the next generation. The default value is `ceil(0.05*PopulationSize)`.
`CrossoverFraction` specifies the fraction of the next generation, other than elite children, that are produced by crossover. The fraction that is not chosen for crossover will suffer mutation. This is an important parameter for tuning because its value can change the results drastically. The default value is `0.8` which is a value that already proved to be the best for several studies [35, 36]. The example `deterministicstudy.m`, which is included in the MATLAB® software, compares the results of applying the genetic algorithm to Rastrigin's function with `CrossoverFraction` set to 0, .2, .4, .6, .8, and 1. The example runs for 10 generations. At each generation, the example plots the means and standard deviations of the best fitness values in all the preceding generations, for each value of the crossover fraction [35]. The example was modified to study the `overlap` function instead, and the results are plotted in Figure 2.13. The lower plot shows the means and standard deviations of the best fitness values over 10 generations, for each of the values of the crossover fraction. The upper plot shows a color-coded display of the best fitness values in each generation. From the plots it is noticeable that, for this fitness function, setting `CrossoverFraction` to `0.8` leads to the best result as well.

Lastly, it is essential to set the stopping criteria options, which determine what causes the algorithm to terminate:
`MaxGenerations` — Specifies the maximum number of iterations for the genetic algorithm to perform;
`MaxTime` — Specifies the maximum time in seconds the genetic algorithm runs before stopping;
`MaxStallGenerations` and `FunctionTolerance` — The algorithm stops if the average relative change in the best fitness function value over `MaxStallGenerations` is less than or equal to `FunctionTolerance`;
`MaxStallTime` — The algorithm stops if there is no improvement in the best fitness value for an interval of time in seconds specified by `MaxStallTime`;
`FitnessLimit` — The algorithm stops if the best fitness value is less than or equal to the value of `FitnessLimit`.

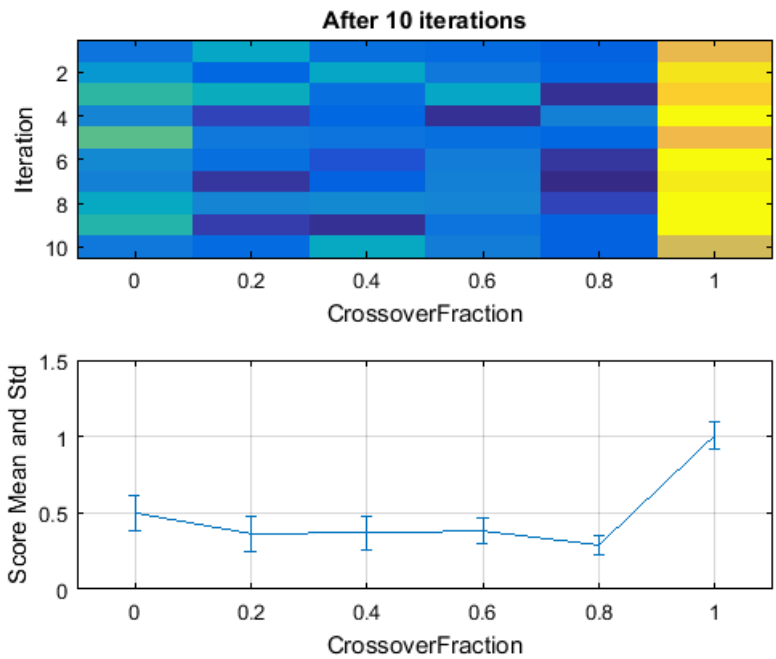

Figure 2.13: Tuning Crossover Fraction.

In our scenario, `FitnessLimit` is equal to zero as it is the minimum value that can be obtained by our fitness function `overlap`. The values of `MaxGenerations`, `MaxTime`, `MaxStallGenerations` and `MaxStallTime` have to be high enough, and the `FunctionTolerance` low enough, to ensure the dominant criteria is to reach the `FitnessLimit`.

2.3.2 Optimization with function `cuckoo_search`

The demo program `cuckoo_search` was written by Yang and Deb [31] for the implementation of a standard version of the CS algorithm. The code uses MATLAB®'s vector capability and is given sequentially according to the process in Figure 2.3.

In order to use `overlap` as the cost function, the code was modified in order to allow more inputs other than the number of nests `n`. The cost function is now also an input, as well as the number of variables, corresponding to `nvars` in the `ga` function. The lower and upper bounds were changed to be equal to `lb` and `ub` values specified in the previous section.

The subfunction `empty_nests` was also modified because after first attempts of implementation, the algorithm, when creating new solutions to fill the empty nests by selective random walks, was not respecting the bounds, generating solutions outside the requested bounds. Therefore, the subfunction `simplebounds`, used for the application of these simple constraints, had to be taken into account and implemented inside this subfunction.
For the optimization options of this algorithm, since the number of variables, i.e. the double of the number of fibres, is often large, the number of nests was doubled from the default value of `25` to `50`.

This is still a low number compared to the corresponding parameter in the GA `PopulationSize`, but the code is extremely time consuming if a larger number of nests is requested. The discovery rate of alien eggs/solutions `pa` was kept with the default value of `0.25`. Regarding the stopping criteria, the tolerance, i.e. the value corresponding to the minimum deviation allowed from the fitness limit of `0`, was reduced to `1.0e-6` and the maximum number of iterations increased to `1.0e10`.

2.3.3 Modification for hybrid composites

Since the objective of this thesis is to study the behaviour of hybrid composites, the original algorithm has to be adapted to handle two different fibres i.e. circles with different radius. The modified code `randgenGA_2fibres` converts the inputs to vectors with two entries, such that `Vol_fibre(1)` and `Vol_fibre(2)` correspond respectively to the fibre volume fraction required for fibre types `1` and `2` with radius `R(1)` and `R(2)`. This will create $n_{fibres1}$ and $n_{fibres2}$. The input parameter `delta` is now defined in a different manner:

$$a = b = \delta \times \frac{R_1 + R_2}{2} \tag{2.18}$$

as well as the `mindist` parameter and the overlapping characteristic function, which, for two different fibres i and j, is defined as

$$f_{ij} = \begin{cases} R_i + R_j + \Delta_{min} \times \frac{R_i+R_j}{2} - d_{ij}, & \text{if } d_{ij} < R_i + R_j + \Delta_{min} \times \frac{R_i+R_j}{2}. \\ 0, & \text{otherwise.} \end{cases} \tag{2.19}$$

This will also imply a new objective function, which will be evaluated with the script `overlap_2fibres`. It can be seen that the adaptation for the hybrid configuration can be performed easily and the code continues to be simple, and it is not necessary to change the output matrix p.

2.4 Statistical characterisation

In this section, some statistical functions and operators commonly used in the literature will be applied to quantitatively characterise the fibre spatial distribution obtained from the `randgenGA`. The results will be compared with those obtained by Melro's [28] method and those obtained with `randgenCS`. Melro [28] MATLAB® scripts for the algorithms `RAND_uSTRU_GEN` and `RAND_uSTRU_GEN-2Fibres` were provided by the author. For the analysis of the single fibre type configuration the parameters used are:

$$R = 0.07 \text{ units of length (u.l.)}$$

$$\delta = 15$$

$$\Delta_{min} = 0.05$$

For the configuration with two different fibre radius, $R_1 = 0.08$ and $R_2 = 0.06$ u.l., and the other parameters will have the same values. For the different fibre volume fractions, for now all runs will have the same amount of each of the two fibres in volume (e.g. if $V_f = 40\%$, it means $V_{f_1} = 20\%$ and $V_{f_2} = 20\%$), which will create more fibres of the smaller radius.

All runs were performed in a notebook computer with an Intel® Core™ i5 2.60 GHz processor and 6GB of RAM memory.

2.4.1 Time

In a first analysis the evaluation of the performance of the difference methods is based on their running time. Tables 2.1 and 2.2 represent the average values of time for five runs with different fibre volume fractions for single fibre type/radius arrangements and for hybrid arrangements with two different fibre types/radius.

	`randgenGA`		`randgenCS`		`RAND_uSTRU_GEN` [28]	
V_f	$\mu(time)$	$\sigma(time)$	$\mu(time)$	$\sigma(time)$	$\mu(time)$	$\sigma(time)$
0.40	5.82	1.24	15.25	2.15	5.25	0.29
0.50	28.77	4.88	290.80	35.85	7.23	1.05
0.60	75.91	19.03	30923.66	7745.48	11.28	1.62

Table 2.1: Average and standard deviations of time in seconds required to run each algorithm for single fibre radius configuration.

	`randgenGA_2Fibres`		`randgenCS_2Fibres`		`RAND_uSTRU_GEN-2Fibres` [28]	
V_f	$\mu(time)$	$\sigma(time)$	$\mu(time)$	$\sigma(time)$	$\mu(time)$	$\sigma(time)$
0.40	6.32	1.04	24.04	3.38	0.32	0.05
0.50	23.38	6.05	482.68	163.71	7.81	2.41
0.60	75.80	18.17	48579.18	10354.53	69.04	46.43

Table 2.2: Average and standard deviations of time in seconds required to run each algorithm for two different fibre radius.

It is clear that the optimization approach with the nature-inspired algorithms takes more time to generate the desired distributions, specially when the fibre volume fraction increases, i.e. when the number of design variables, given by the number of fibres, increases. Even so, the genetic algorithm performs much better in terms of time than the cuckoo search method, that could only reach the 60% fibre volume fraction in more than 8 hours in average.

The main problem of this time increase with the number of design variables is the way it limits the parameter δ defining the size of the RVE. Although the size of the area of interest also increases, the stochastic processes in this nature-inspired algorithms have difficulties in find an optimum point with a big set of design variables. However, since the RVE will be transformed into a finite element mesh, a

bigger size involving more fibres would create a very heavy mesh not capable of great refinement.

For the hybrid configuration the `RAND_uSTRU_GEN-2Fibres` denoted some flaws in achieving the 60% fibre volume fraction, failing to reach this required volume fraction 5 times out of 10 runs (only the five runs that the volume fraction was achieved counted for the average and standard deviation tabled), regardless of continuing to be faster if a 40% or 50% fibre volume fraction is requested. However, composite materials normally have fibre volume fractions between 55 and 65%, thus `randgenGA` performance is the best concerning the generation of RVE for fibre-hybrid composites.

2.4.2 Voronoi polygon areas and neighbouring distances

A Dirichlet tessellation is defined as a subdivision of a region, determined by a set of points, where each point has associated with it a region that is closer to it than to any other. These regions are named Voronoi cells. The aggregate of all such regions, constitutes the Dirichlet tessellation in a plane. Figure 2.14(a) shows an example of such tessellation for a random distribution of points while Figure 2.14(b) provides the tessellation for a periodic square distribution. Each polygon represents a Voronoi cell.

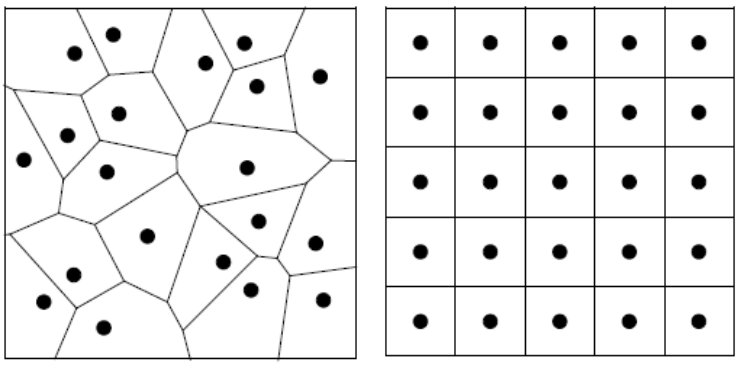

(a) Random distribution (b) Periodic distribution

Figure 2.14: Voronoi cells [28].

A Voronoi cell immediately identifies the region of immediate influence for each fibre. The number of neighbouring cells also provides insight to the clustering that the fibre belongs to or if it is an isolated fibre.

The standard deviation of the areas of the Voronoi polygons can be calculated to infer about the quality of the spatial distribution of the fibres. For a periodic distribution, for example, the standard deviation is null as all Voronoi cells are equal in area.

With the definition of a Voronoi cell for each fibre, one can also calculate the standard deviation of the average of the distances between fibre centres to the neighbouring fibres. A neighbouring fibre is one which shares a side of the Voronoi polygon with the fibre of interest. This measure functions the same way as the previous providing an insight into the degree of clustering or spacing between the fi-

bres. A value close to zero indicates that the fibres are all at an approximately equal distance from each other (or, if the value is 0, exactly at the same distance as is the case of periodic distributions).

For this test, following Melro [28]'s procedures, the coefficient of variation will be used instead of the simple standard deviation, which is defined according to Equation (2.20).

$$\rho(x) = \frac{\sigma(x)}{\mu(x)} \tag{2.20}$$

The variable x represents the areas of the Voronoi cells or the distances to neighbouring fibres corresponding to the spatial fibre distribution in analysis. Table 2.3 shows the average of five runs for the coefficient of variation of both areas of Voronoi cells and neighbouring distances for each method. Note that periodic distributions have ρ_A = ρ_D = 0. This statistical spatial descriptor will only be applied to single fibre type configurations, as the Voronoi polygons only make sense if all the fibres have the same radius (with different radius the distances can always be lower for two fibres having the minimum of the two radius).

	`randgenGA`		`randgenCS`		`RAND_uSTRU_GEN` [28]	
V_f	ρ_A	ρ_D	ρ_A	ρ_D	ρ_A	ρ_D
0.40	0.178	0.235	0.230	0.276	0.204	0.233
0.50	0.124	0.226	0.148	0.211	0.208	0.217
0.60	0.124	0.201	0.108	0.164	0.124	0.180

Table 2.3: Coefficient of variation for Voronoi polygon areas and distances to neighbouring fibres.

For higher fibre volume fractions, the fibres will be more compacted, meaning that the fibres will have less chance to move around. This explains why the coefficients values decrease when the fibre volume fraction increases. This adds difficulties to the stirring step of `RAND_uSTRU_GEN`, causing the performance for the higher fibre volume fractions to be worse than `randgenGA` performance. For the lower fibre volume fractions `randgenCS` has the highest values for both coefficients of variation.

2.4.3 Examples of generated RVE geometries

Examples of achieved geometries from the three different algorithms for 40, 50 and 60% fibre volume fractions are illustrated in Figures 2.15-2.20 for comparison, both for arrangements with one fibre type and two fibre types. An example for $V_f = 65\%$ is also shown in Figure 2.21 for `randgenGA` and `RAND_uSTRU_GEN` to prove the new code's capability of reaching high fibre volume fractions.

From the distribution plots it is possible to take conclusions as well about the performance of the algorithms. All the algorithms use very random processes, although the nature-inspired methods clearly have more uncertain ways of finding the optimal design. This will cause, especially for $V_f = 40\%$ (Figures 2.15 and 2.18), fibre clusters when there are matrix rich areas, i.e. when there is space for more distance between fibres. Since the optimized objective function reaches its goal value, thus stopping the

algorithm, when the minimum distance allowed is satisfied, even if all the fibres were close by this minimum distance and there was lots of space without fibres, the algorithm would have found its optimum. This can be easily fought by increasing the Δ_{min} parameter. However, we are trying to portray as much as possible real UD composite materials, where we know the fibres are randomly displaced, and so we must take into account the possibility of fibre aggregation creating matrix rich areas.

Another thing noticed by the spatial arrangements found was the tendency to create too many fibres crossing the RVE boundaries or close to it, more particularly for `randgenCS`, which is of course necessary when high fibre volume fractions are required (case of $V_f = 60\%$), but can create problems when generating the finite element mesh, issues that will be discussed later in this work.

The numerical results registered in the upper part of each image represent the number of iterations of each algorithm and the real fibre volume fractions achieved, which is always approximate to the one required, but not exactly the same because the number of fibres must always be an integer number, as already explained, due to the need of imposing periodic boundary conditions. Note that for the genetic algorithm the iterations, called generations, represent `Generations*PopulationSize` function evaluations, and for the cuckoo search algorithm the iterations are equal to the number of function evaluations, thus the discrepancy between them. For Melro's [28] algorithm, each iteration passes through the three steps and corresponds to about 200 attempts of fibre placing for $V_f = 40\%$, 10000 attempts for $V_f = 50\%$ or 30000 attempts for $V_f = 60\%$, though the number of attempts is extremely variable.

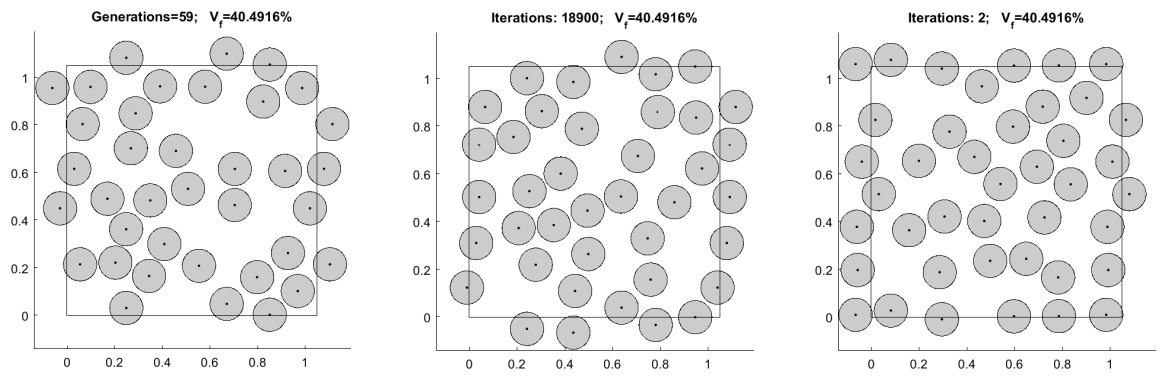

(a) `randgenGA` (b) `randgenCS` (c) `RAND_uSTRU_GEN`

Figure 2.15: Single fibre configuration: $V_f = 40\%$.

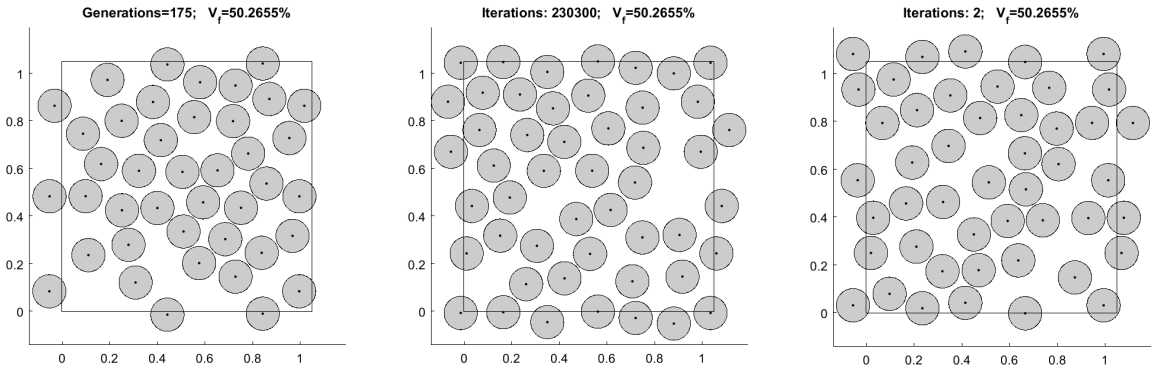

(a) `randgenGA` (b) `randgenCS` (c) `RAND_uSTRU_GEN`

Figure 2.16: Single fibre configuration: $V_f = 50\%$.

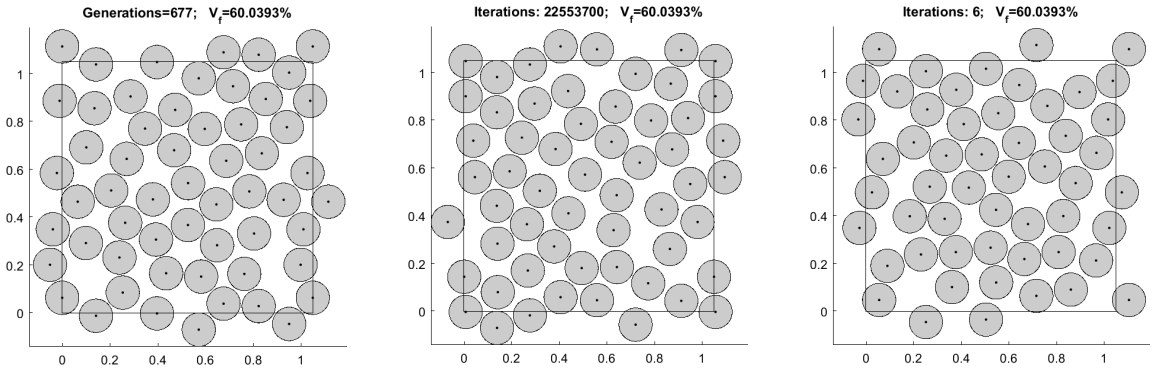

(a) `randgenGA` (b) `randgenCS` (c) `RAND_uSTRU_GEN`

Figure 2.17: Single fibre configuration: $V_f = 60\%$.

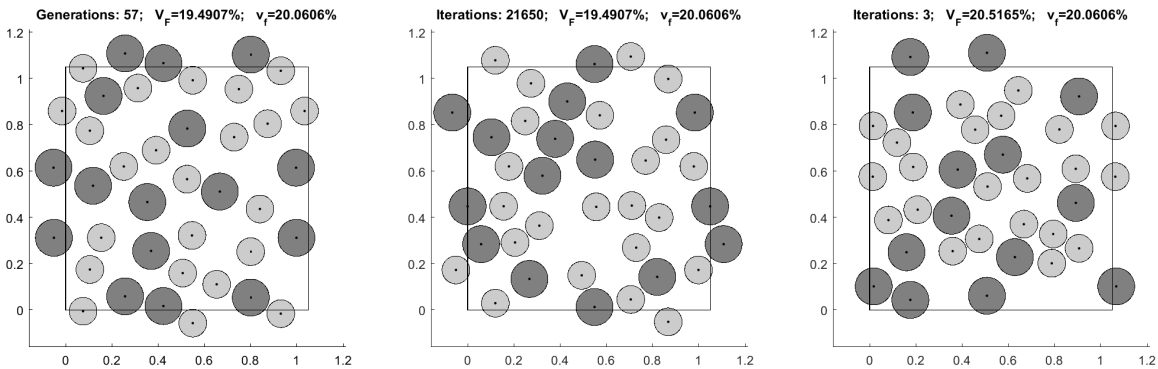

(a) `randgenGA` (b) `randgenCS` (c) `RAND_uSTRU_GEN`

Figure 2.18: Fibre-hybrid configuration: $V_f = 40\%$.

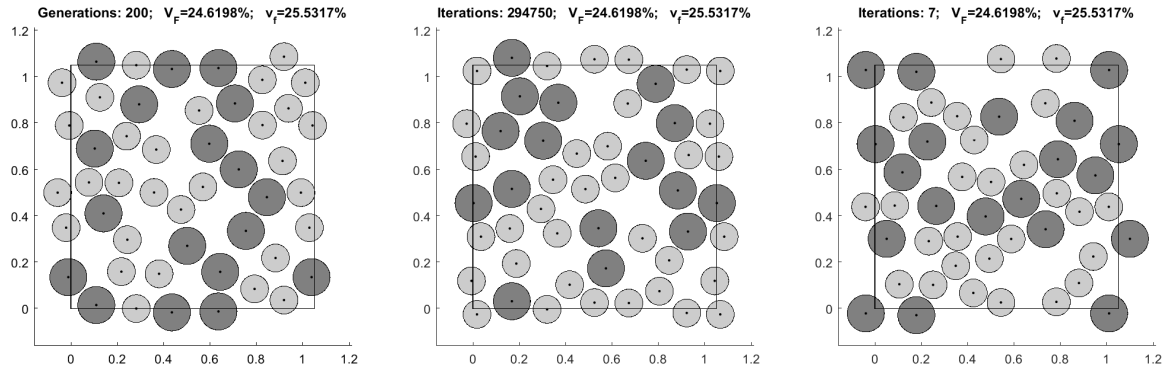

(a) randgenGA (b) randgenCS (c) RAND_uSTRU_GEN

Figure 2.19: Fibre-hybrid configuration: $V_f = 50\%$.

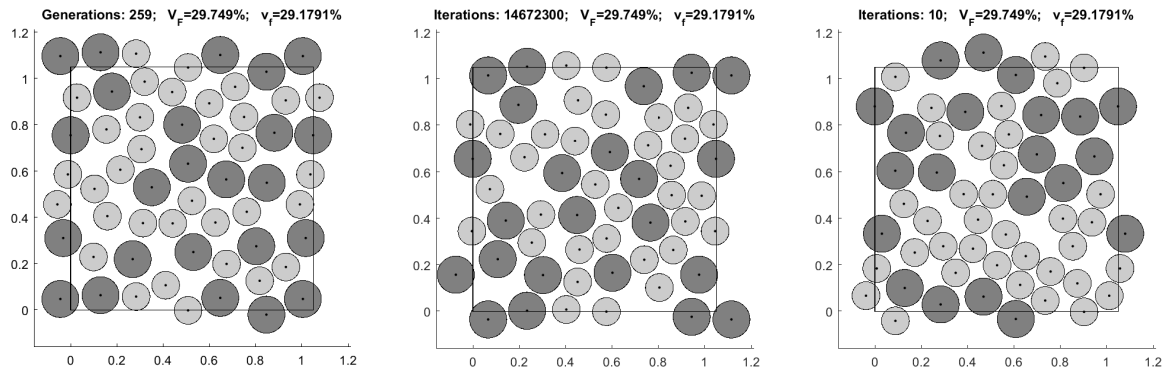

(a) randgenGA (b) randgenCS (c) RAND_uSTRU_GEN

Figure 2.20: Fibre-hybrid configuration: $V_f = 60\%$.

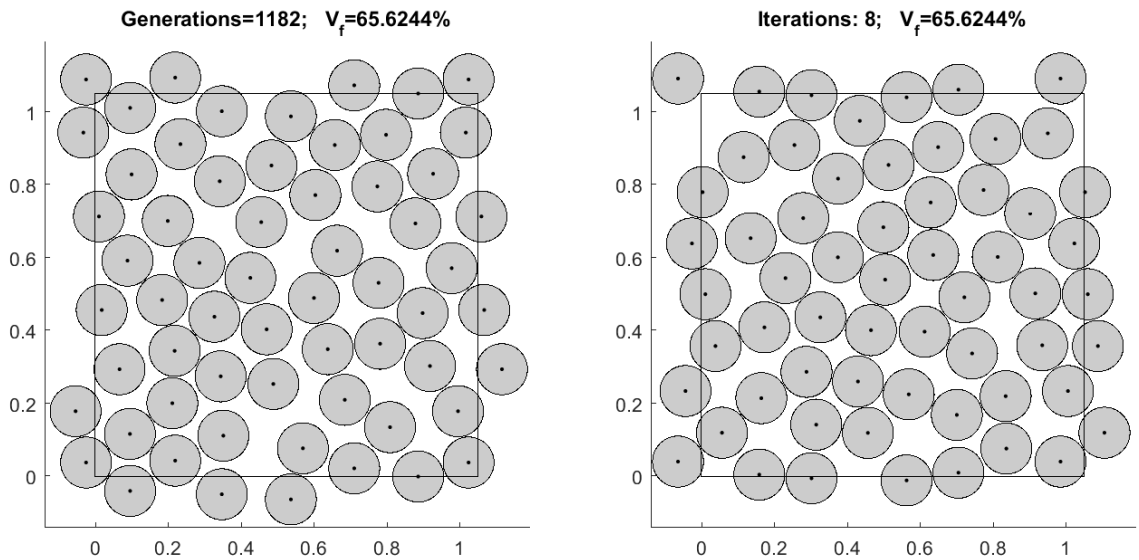

(a) randgenGA (b) RAND_uSTRU_GEN

Figure 2.21: Single fibre configuration: $V_f = 65\%$.

Chapter 3

RVE equivalent properties

This Chapter aims to present how the mesh is created for FEA and the software needed to compute the homogenized properties of the generated RVE geometries. It starts by a brief explanation of the homogenization theory, which is after implemented with PREMAT, software developed by Guedes and Kikuchi [25], which uses FEM to compute the material equivalent properties. Thus, the fibre random distributions found with `randgenGA` must be transformed into finite element 3D grids. Some examples of the generated meshes and correspondent PREMAT computations will be addressed below.

3.1 Homogenization theory

Due to the material heterogeneity created by the presence of matrix and fibres, it is extremely difficult to analyse composites at one structural-material level due to the extraordinarily fine discretization required. To overcome this difficulty, one looks for an equivalent material model capable to characterize the average mechanical behaviour as well as represent the effect of the composite material heterogeneities, without representing each individual microstructure. The homogenization theory is a mathematical theory well described in literature allowing the representation of this kind of engineering models [25, 37–41]. The method enables the computation of local stress and strain distribution based on the analysis of an RVE characterizing the composite material microstructure. A brief explanation addressing Guedes and Kikuchi's [25] approach will be now presented.

Consider a composite material formed by the spatial repetition of a very small base cell, of order ε, made of two different materials as shown in Figure 3.1. If the macroscopic body is subjected to load and boundary conditions, the resulting deformation and stresses will rapidly vary from point to point because of the repetition of microscopic base cells producing heterogeneity. In other words, with the high level of heterogeneity within the material, these quantities also vary rapidly within a very small neighbourhood ε of a given point x. Thus it is reasonable to assume that all quantities have two explicit dependences: the macroscopic level x, and the microscopic level x/ε, i.e. for a general function g, $g = g(x, x/\varepsilon)$. Due to the periodic nature of the microstructure, the dependence of a function on the microscopic variable

$y = x/\varepsilon$ is also periodic.

Figure 3.1: Periodic composite structure.[25]

Considering the problem of the deformation of a solid body Ω^ε with no holes like the RVE's we are studying, the body forces f, traction t on the boundaries and the elastic constants will vary within a small cell of the composite, thus being all functions of x and $y = x/\varepsilon$. Therefore, the solution u^ε for this problem should also depend on both x and $y = x/\varepsilon$, making it reasonable to claim that u^ε can be expressed as an asymptotic expansion, with respect to the parameter ε:

$$u^\varepsilon(x) = u^0(x,y) + \varepsilon u^1(x,y) + \varepsilon^2 u^2(x,y) + ..., \quad y = x/\varepsilon. \tag{3.1}$$

To find the homogenized elastic constants we must find an equation that can describe the macroscopic equilibrium. These homogenized constants should be such that the corresponding equilibrium equation reflects the mechanical behaviour of the microstructure of the material without the need to explicit the microscale parameter ε.

The equation for the homogenized properties D is reached

$$D_{ijkl} = \frac{1}{|Y|}\int_Y \left(E_{ijkl} - E_{ijpm}\frac{\partial \chi_p^{kl}}{\partial y_m} \right) dY \tag{3.2}$$

where $\chi^{kl} \in V_Y$ is the solution of the local problem equilibrium equation:

$$\int_Y E_{ijpm}\frac{\partial \chi_p^{kl}}{\partial y_m}\frac{\partial v_i(y)}{\partial y_j} dY = \int_Y E_{ijkl}\frac{\partial v_i(y)}{\partial y_j} dY \quad \forall v \in V_Y \tag{3.3}$$

For further knowledge on how to reach these formulae see [25] and for other approaches on the homogenization theory see [41].

3.2 Implementation using PREMAT

Following the homogenization theory, Guedes and Kikuchi [25] developed a software for material preprocessing named PREMAT to calculate the homogenized elastic constants of the RVE through Equation (3.2) using FEM. The program reads the constituents of the basic cell, reads the material elastic constants of each constituent, performs the homogenization computations by simulating tensile and shear loading tests on the input RVE and finally rotates matrix D to the coordinate system in which the element stiffness matrices are computed. The goal is to posteriorly combine this program with the material post-processing program POSTMAT which computes local distribution of stresses and strains

within the microscopic level. In Chapter 4 the stress analysis will be conducted using POSTMAT.
In order to use PREMAT we first need to create a finite element mesh to the transverse random fibre arrangement obtained from the previous chapter generator. In this section we address the construction of the three-dimensional mesh with an open-source generator created by Geuzaine and Remacle [42] called Gmsh, and how to transfer the generated grid to PREMAT.

3.2.1 Generating finite element mesh with Gmsh

To proceed with the computational analysis of the mechanical behaviour of the UD composite material, it is now necessary to resort to finite element methods. For the mesh generation, the chosen program was Gmsh, since it is an open-source program with a built-in CAD engine capable to design a geometry through a `.geo` file with its own scripting language, adding the ability to create a three-dimensional mesh from the command line. This way, there is no need to open the program window when a new mesh is generated and outputted through a `.msh` file. More informations about the program's capabilities, scripting language and mesh generating algorithms can be seen in [42] or in the software reference manual [43].

The idea is to create a two-dimensional mesh for the transverse section obtained with `randgenGA` and then build the three-dimensional mesh by simple extrusion with only one element in depth. For that purpose, the MATLAB® function `generate_geo` was written, which transforms the circle distribution found into a `.geo` file to serve as input in Gmsh.

The generation of the geometry starts with the point placing. The points are defined through their coordinates (x, y, z) and a fourth coordinate is added regarding the mesh element size. This fourth coordinate is represented by the element size parameter `lc` that must be equal for all points in order to create a uniformly sized mesh. In our case, a circle must be defined by at least two radial points in the circumference separated by an arc of π radians, besides of course the centre point. For the circles crossing the boundaries of the RVE, it is necessary to specify the points where the circumferences intersect the edge or edges of the square that limits the RVE boundaries, since the only part of the circle we represent is the one inside that square. Since all the points are in the same transverse section $z = 0$ for all points. So, the coordinates (x, y) of the centre points for each circle come directly from the output vector p, as well as their radius R. Then, for a circle fully inside the RVE, four points are generated at the north, west, south and east positions along the circumference with respect to the circle centre as shown in Figure 3.2. For a circle that is cut by the edges of the area of interest, at least the two intersecting points are needed, or more if the arc described between the two points is greater than π rad. The four corner points of the RVE must also be defined. Each point is assigned a number i and generated with the command `Point(i)`. All consecutive points are then joined with the `Circle` command if the path between them is ought to be part of a circumference (circular path) or with the `Line` command if the path is part of the edges (straight path). To form an arc of circumference with the `Circle` command we need

to specify the start point, the centre point and the end point of the arc, to generate a straight line with the `Line` command we just need the start and end points of the line. This lines will also have a number assigned for each one.

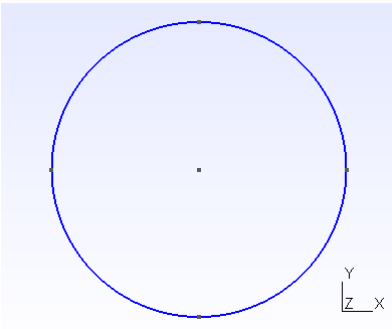

Figure 3.2: Circular form in Gmsh.

The next step is to connect the generated lines of type `Circle` and `Line` in order to define the corresponding surfaces for the fibres and the surface for the matrix. The `LineLoop` command can join the lines necessary to form a surface, that must be closed but can have holes, which is the case of the matrix surface (the holes will be occupied by the surfaces representing the fibres). One line loop will be created for each circle or partial circle and one line loop will be created for the matrix. The matrix loop has to account for the circles crossing the edges, i.e. it cannot be simply created by connecting the four corner points of the RVE, it needs to contour the circular forms attached to the limit lines, as shown in Figure 3.3 for a simple configuration with one fibre in the middle and the other distributed by the four corners. The loop along with the hole created by the introduction of the fibre in the middle define the matrix surface.

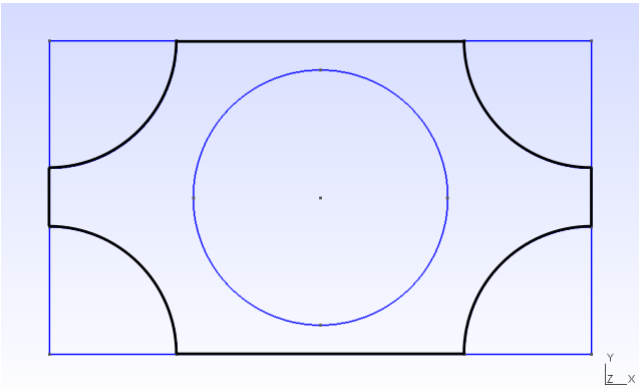

Figure 3.3: Matrix loop (bold black line).

Once all surfaces are defined, we have the two-dimensional geometry completely designed. To proceed to the three-dimensional geometry, the surfaces are extruded along the z direction to create volumes. The extrusion depth does not need to be significant since, as we said, the mesh is only intended to have one element along this direction. From the volumes created Gmsh has the option to create physical entities for the posterior assignment of materials to each volume.

After the geometry is created and the volumes are well defined, the finite element mesh is generated by calling Gmsh on the command line. As the volumes were created through extrusion, the 2D mesh is first generated in an unstructured way, and can be composed by irregular triangles or quadrangles. The extrusion copies this surface mesh along the z direction and unites the two sections in a structured way, forming tetrahedra, prisms, hexahedra or pyramids. Gmsh also has the option to apply an elliptic smoother to the finite element mesh. The generated mesh results in a `.msh` file, where the program writes the coordinates of the nodes and their combination into elements.

3.2.2 Exporting the mesh to PREMAT

To compute the homogenized elastic constants, the 3D mesh generated in Gmsh must be exported to PREMAT workspace. PREMAT is only capable of working with 8-node and 20-node hexahedral elements and 4-node and 10-node tetrahedral elements, thereby we will only generate meshes with these types of elements.

To accomplish the homogenization for the generated mesh in PREMAT we first need to convert the `.msh` file generated by Gmsh into an input text file for the PREMAT mesh module MESH3D, where the program applies the periodic boundary conditions necessary to conduct the analysis. The function `convert` was written in MATLAB® with that purpose. It copies the nodes and elements information and adds the material properties (Young's modulus and Poisson's ratio) to both fibres and matrix. The fact that the three-dimensional grid generated by Gmsh has symmetry concerns between opposite surfaces, with the nodal positions of the elements situated on the boundary surfaces matching across RVE thickness, width and height, made the process easier. The only problem found was in the nodal sequence for the elements, that had to be rearranged for some cases. The node ordering for tetrahedral elements and hexahedral elements of both meshing modules are illustrated in Figures 3.4 and 3.5.

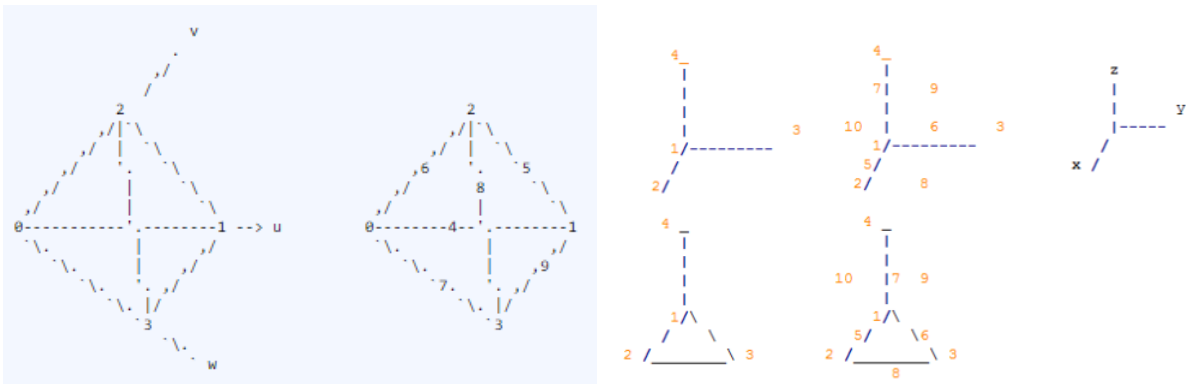

(a) Gmsh [43] (b) PREMAT

Figure 3.4: Node ordering for tetrahedra.

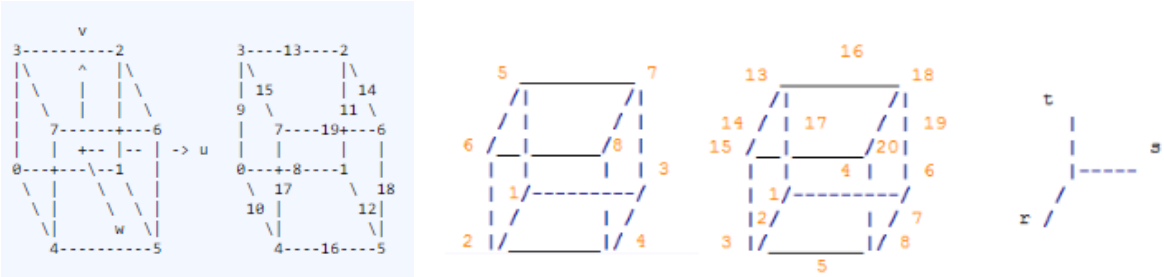

(a) Gmsh [43]

(b) PREMAT

Figure 3.5: Node ordering for hexahedra.

It is noticeable that the node ordering is the same just for the 4-node tetrahedron, thus for the other element types the nodes coming from the `.msh` file must be reordered to become in agreement with PREMAT node sequence. Consider that the Gmsh ordering starts with 1 instead of 0, such that in Figures 3.4(a) and 3.5(a) the 0 becomes 1, 1 becomes 2, and so on, to be in accordance with the PREMAT counting. The rearrangement Gmsh $\rightarrow$ PREMAT[1] is:

- For the 10-node tetrahedron: 1-5, 9 and 10 stay in the same position; 7 $\rightarrow$ 6, 8 $\rightarrow$ 7, 6 $\rightarrow$ 8.
- For the 8-node hexahedron: 1, 2, 5 and 6 stay in the same position; 4 $\rightarrow$ 3, 3 $\rightarrow$ 4, 8 $\rightarrow$ 7, 7 $\rightarrow$ 8.
- For the 20-node hexahedron: 1 stays in the same position, 9 $\rightarrow$ 2, 2 $\rightarrow$ 3, 10 $\rightarrow$ 4, 12 $\rightarrow$ 5, 4 $\rightarrow$ 6, 14 $\rightarrow$ 7, 3 $\rightarrow$ 8, 11 $\rightarrow$ 9, 13 $\rightarrow$ 10, 16 $\rightarrow$ 11, 15 $\rightarrow$ 12, 5 $\rightarrow$ 13, 17 $\rightarrow$ 14, 6 $\rightarrow$ 15, 18 $\rightarrow$ 16, 19 $\rightarrow$ 17, 8 $\rightarrow$ 18, 20 $\rightarrow$ 19, 7 $\rightarrow$ 20.

With the output `.msh` file of Gmsh finally converted to an input text file, MESH3D is called to run and the periodic boundary conditions between the nodes in opposite surfaces of the RVE are assigned. This creates the input file for PREMAT `boneco.txt` which is the only file PREMAT needs to finally compute the homogenized properties of the composite material.

To assure that Gmsh and PREMAT can indeed couple to perform homogenization through FEM, a compatibility study between the two programs will be addressed.

Compatibility between Gmsh and PREMAT

In order to validate the use of Gmsh we need to study the compatibility between the generated mesh and PREMAT software. To do so, we will use PREMAT CAD capabilities of generating predefined simple cells with unitary volume for an hexagonally periodic distribution (RVE type 8) and a quadratic periodic distribution (RVE type 212) of fibres and compare the results obtained in the homogenization for identical cells generated by Gmsh (geometries created in Gmsh illustrated in Figure 3.6).

The PREMAT mesh generator uses a mesh refinement parameter `ian` to manipulate the mesh element

[1] The arrow means that the node number i in Gmsh becomes the node number j to the PREMAT meshing module

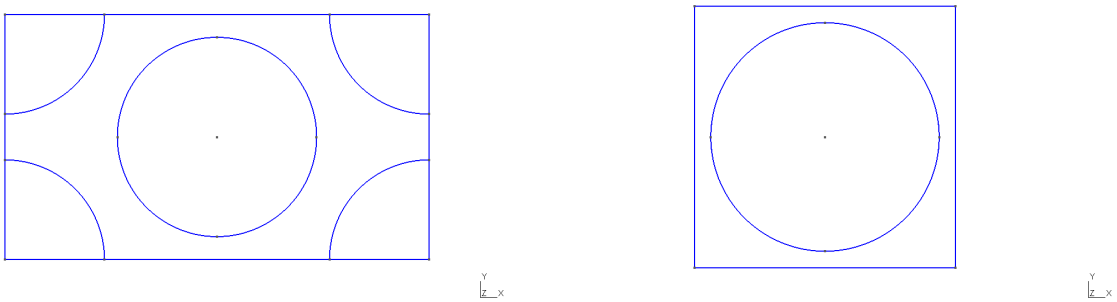

(a) RVE type 8 (b) RVE type 212

Figure 3.6: Geometries generated in Gmsh for a fibre volume fraction of 60%.

size. The number of nodes per element is given by `node` and all elements are formed in a structured way, unlike Gmsh. The idea is to compare the homogenized constants computed through a mesh created within PREMAT and, for the same geometry, a mesh created in Gmsh. Therefore, the number of elements created for each mesh needs to be as close as possible. Starting by a convergence study for the homogenized constants matrix D for the quantity `ian` and the corresponding number of elements created, the values for this parameter where chosen. Then, the mesh refinement parameter of Gmsh, `lc`, was manipulated so that the number of elements generated in Gmsh would be equal or close to the number of elements obtained with the `ian` values selected. The results for the mesh refinement parameters are registered in Table 3.1 for fibre volume fractions of 40, 50 and 60%. Notice that having 4 or 10 nodes per element always represent tetrahedral elements, i.e. it does not change the number of elements, only the number of nodes. The same goes for the hexahedral elements that can be composed by 8 or 20 nodes.

V_f	RVE type	Nodes per element	PREMAT		Gmsh	
			`ian`	N. of elements	`lc`	N. of elements
0.4	8	4/10	7	8820	0.030	8778
		8/20	7	1764	0.030	1660
	212	4/10	6	9600	0.029	9672
		8/20	6	1920	0.027	1912
0.5	8	4/10	5	7980	0.032	7776
		8/20	5	1596	0.030	1699
	212	4/10	4	7020	0.034	7188
		8/20	4	1404	0.030	1558
0.6	8	4/10	4	11880	0.026	12066
		8/20	4	2376	0.025	2221
	212	4/10	4	17100	0.022	17064
		8/20	4	3420	0.020	3425

Table 3.1: Selection of mesh refinement parameters

Having established the mesh refinement parameters for both programs, we can now finally compare the homogenization results as given by PREMAT computations for the two different generated meshes. The

finite element grids generated for a fibre volume fraction of 60% are shown in Figure 3.7 for the RVE type 8 configuration and in Figure 3.8 for the RVE type 212 configuration.

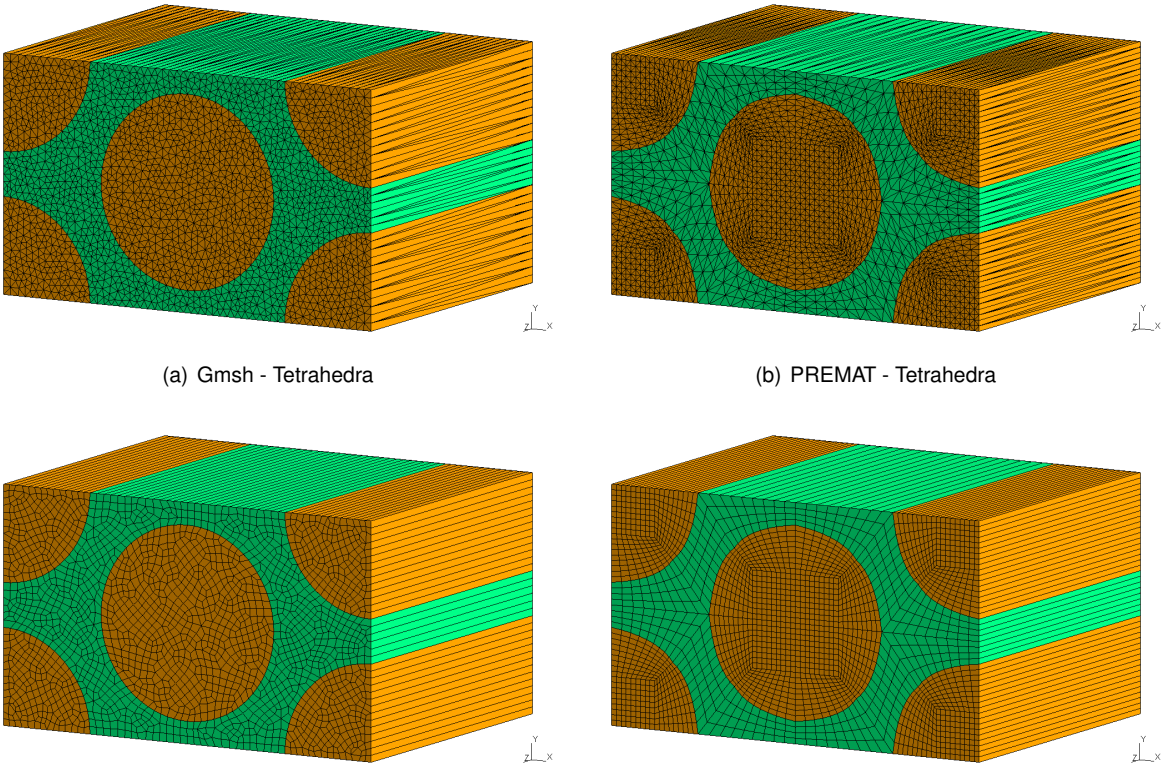

(a) Gmsh - Tetrahedra

(b) PREMAT - Tetrahedra

(c) Gmsh - Hexahedra

(d) PREMAT - Hexahedra

Figure 3.7: Meshes obtained for RVE type 8.

From this images we can clearly spot the differences between the generated meshes. While PREMAT creates structured grids, but with a clear variation of the mesh element size (elements in the fibres are much smaller than those in the matrix), the grid generated by Gmsh is of stochastic nature but with the element size almost uniform, providing more elements in the matrix part of the RVE.

The comparison for the homogenized properties was made regarding the diagonal of the D matrix computed by PREMAT and written in the program's output text file `prhoutput`, matrix from where the program takes the Young's and shear moduli as well as the Poisson's ratio of the equivalent homogenized material. The option of using 10-node tetrahedra and 20-node hexahedra was disregarded since it would create too many nodal points and cause the program to run much slower or not even run at all by overcoming the memory size available. The material properties for the fibre and matrix used in these tests were:

$$
\begin{aligned}
E_f &= 290\ GPa,\ \nu_f = 0.35 \\
E_m &= 4.5\ GPa,\ \nu_m = 0.40
\end{aligned}
\tag{3.4}
$$

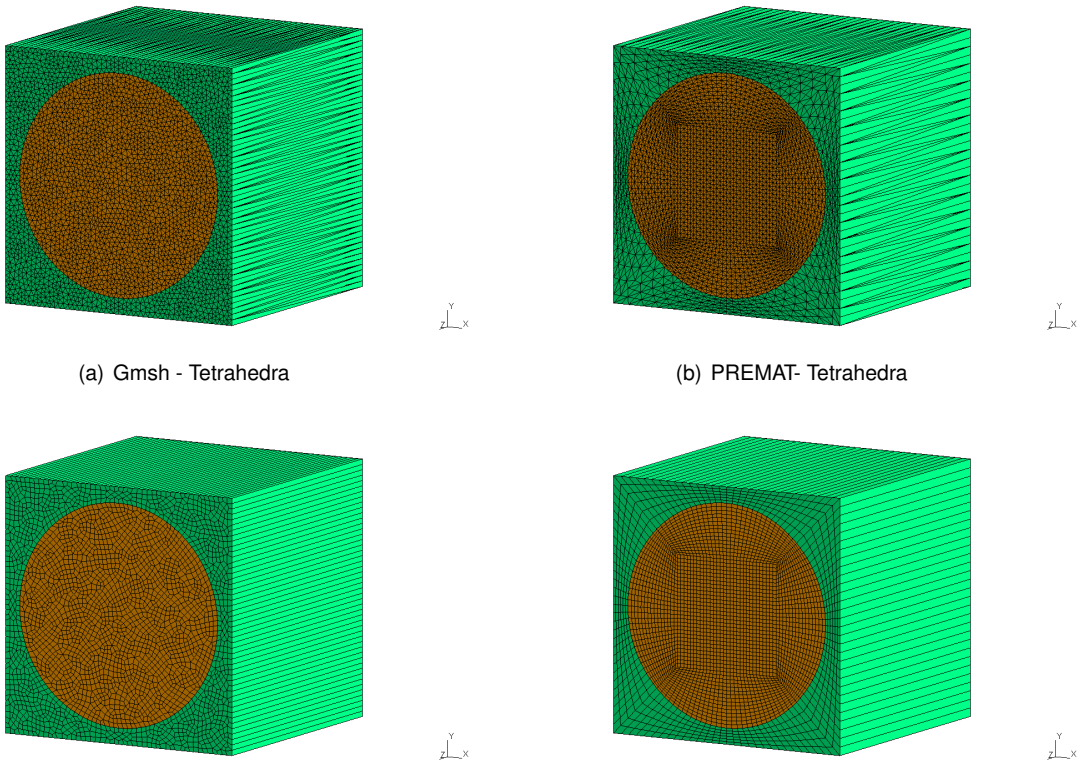

(a) Gmsh - Tetrahedra

(b) PREMAT- Tetrahedra

(c) Gmsh - Hexahedra

(d) PREMAT - Hexahedra

Figure 3.8: Meshes obtained for RVE type 212.

where E_f, ν_f represent respectively the Young's modulus and the Poisson's ratio of the material of the fibre, and E_m, ν_f the corresponding properties for the matrix material. The tests were conducted with the parameters specified in Table 3.1 for both 4-node and 8-node element mesh configurations with 40, 50 and 60% of fibre volume fraction. The results for the diagonal of the homogenized constants matrix proved to be similar for the types of RVE generated by both meshing modules, with the maximum deviations obtained to be of 1.96%, 2.28% and 2.56% for the hexagonally periodic configuration (RVE type 8) for the sixth entry of the diagonal (corresponding to the shear modulus G_{12}) at the three required values of the fibre volume fraction. All the other results obtained had deviations of less than 1%, thus making it reasonable to validate the use of Gmsh as the mesh generator for the study of the generated RVE's.

However, for more complex geometries, if quadrangular elements are required to the Gmsh program the mesh generating algorithm does not guarantee that all elements will be quadrangular, leaving some in the triangular form. An example of this situation is shown in Figure 3.9. This will create problems with PREMAT, which requires all elements to be the same type, with only two hypothesis: hexahedral elements or tetrahedral elements. Since the generated RVE's will be complex due to the stochastic distribution of a considerable number of fibres, to assure all the elements have the same form, i.e. to assure that the homogenization is well implemented in PREMAT, from now on we will only generate tetrahedral meshes.

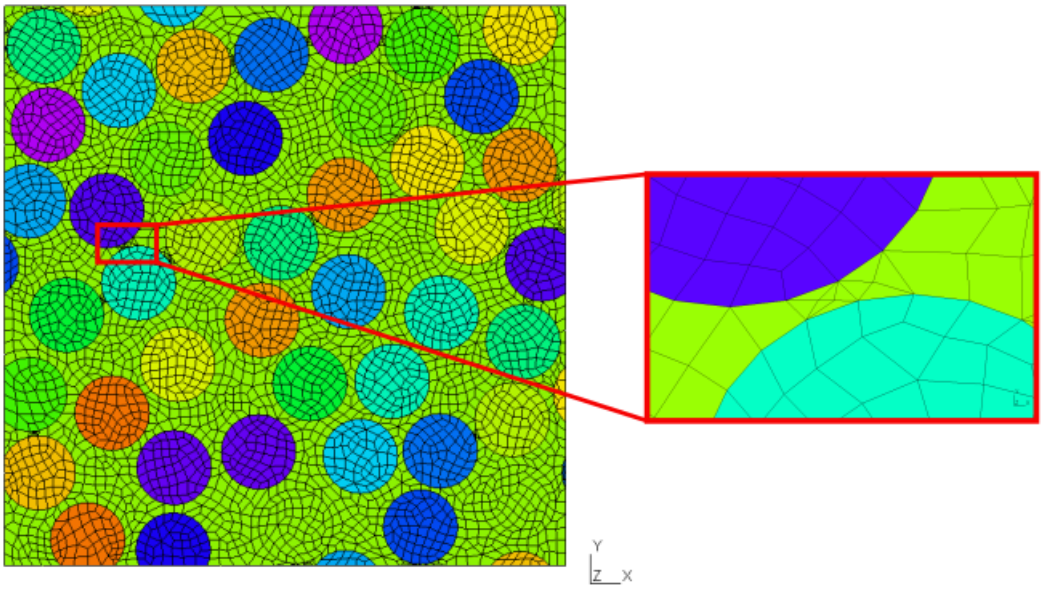

Figure 3.9: Gmsh meshing error generating quads.

3.3 Examples

In this section some examples of generated finite element meshes will be presented. The influence of parameters in the homogenized properties will be studied, more specifically the ones concerning the RVE size and the mesh element size, δ and `lc`. A different set of random distributions will be tested, along with a periodic arrangement, to understand how the PREMAT program behaves for the generated RVE geometries and also to serve as a way to validate the transverse randomness reinforcement generator developed in Chapter 2.

3.3.1 Parametric studies

The first parameter analysed was the one defining the mesh element size in Gmsh input `.geo` file, `lc`. This parameter will be given by a fraction of the side length a of the squared RVE. The tests considered the time spent in mesh generation (Gmsh), assignment of periodic boundary conditions (MESH3D) and homogenization (PREMAT), along with the number of nodes and elements generated and the convergence for the material constants matrix D. This convergence will be represented by the average deviation of the diagonal entries of this matrix for the previous larger value of `lc`. All tests were performed for the same RVE geometry with $V_f = 60\%$, $\delta = 15$ and the results are shown in Table 3.2. Obviously, the values for the matrix and fibre properties are the same for all runs.

The principal value taken into account was that defining the convergence for the homogenized constants. We can see that the first value to have a deviation less than 1% from the previous one is `lc`=$a/40$. From there we see that decreasing the element size leads to more time spending computations, although it does not compensate in the equivalent properties calculated. Therefore, the chosen value for the element size parameter `lc` to use when generating the FE mesh through Gmsh is `lc`=$a/40$.

lc	Time (s)			Number of elements	Number of nodes	D matrix average deviation (%)
	Gmsh	MESH3D	PREMAT			
$a/20$	7.4277	0.4841	5.6037	2362	6792	-
$a/25$	6.9792	0.3899	9.4255	3036	8724	4.31
$a/30$	8.0890	0.4730	14.6833	3840	11082	1.12
$a/35$	9.3916	0.5975	22.1061	4828	13992	1.02
$a/40$	9.8213	0.6651	30.7623	5648	16398	0.36
$a/50$	15.3999	1.4039	72.4288	7844	22854	0.52
$a/60$	19.2456	1.7712	150.7476	10866	31806	0.36

Table 3.2: Parametric study for mesh refinement parameter `lc`

Having specified the element size parameter the influence of the RVE size parameter δ will be studied in a similar manner. However, this parameter influences the most the time spent in generating the random fibre distribution with `randgenGA` so, only this time will be taken into consideration for these runs, along with again the deviation caused by the size of the RVE on the computed equivalent properties. The elastic constants of fibres and matrix and the radius of the fibres is kept constant during all runs, with $V_f = 60\%$.

δ	`randgenGA` time (s)	D matrix average deviation (%)
10	7.9534	-
12	17.9122	9.71
14	78.1547	4.05
16	110.4126	3.54
18	607.3614	3.67
20	988.8835	4.81

Table 3.3: Parametric study for RVE size parameter δ

It can be seen how the time spent is a major concern in the implementation of the genetic algorithm for the generation of the transverse randomness. We can see that the values for the homogenized elastic properties of the composite change more with the variation of the size of the RVE, but since we are at the GPa levels changes of 4% are not that significant and can be also explained by the completely different fibre arrangements we get when running `randgenGA` multiple times, which will be shown in Section 3.3.2. This way, we can see that the average deviation is similar for values of δ above 14. As expected, the time changes drastically though, which leads to the statement that it does not pay to have high δ values for our case. The size parameter used will be the one which has been already considered in the previous examples, $\delta = 15$.

3.3.2 Random fibre arrangements

In order to understand how the PREMAT program behaves for RVE geometries created from `randgenGA`, ten tests were conducted with different random fibre distributions and the equivalent properties computed were compared. The runs were made using fibre volume fractions of 40, 50 and 60% and a regular fibre

arrangement was taken into account for each one. All tests use the parameters chosen above and the fibre and matrix properties utilized were the same of Equation (3.4) but the fibres, although with the same properties, were assigned two different radius, as if we were leading with two different materials for the fibres. The resulting data in Table 3.4 correspond to the average number of nodes and elements for the ten random distributions obtained, the number of nodes and elements obtained for a regular fibre distribution and the average deviation of each of the six entries of the diagonal of the homogenized constants matrix D from the ten different random distributions to the ones obtained using the regular distribution, i.e.

$$\sigma(D_{ii_j}) = \frac{D_{ii} - D_{ii_j}}{D_{ii}}, \quad i = 1, ..., 6, \; j = 1, ...10. \tag{3.5}$$

where D_{ii} are the values for the diagonal entries for a regular distribution and D_{ii_j} are the same values for each of the ten random distributions found. Thereby, the last column represents the average of each of these ten deviations $\bar{\sigma}(D_{ii_j})$ for each diagonal entry of D. Notice that the first three entries of the matrix D diagonal are related to the tensile properties of the composite, respectively E_{11}, E_{22}, E_{33}, and the last three entries represent the shear properties G_{23}, G_{13}, G_{12}[2].

	Random distributions		Regular distribution		$\bar{\sigma}(D_{ii_j})$
V_f	N. of nodes	N. of elements	N. of nodes	N. of elements	(%)
0.4	15387	5307	15072	5192	6.11 -0.57 -0.08 2.93 -6.41 10.13
0.5	15621	5338	15216	5236	-7.87 3.12 -0.19 1.90 -14.26 -12.46
0.6	16543	5700	15414	5302	-1.58 -3.29 -0.46 -12.88 -12.01 -33.01

Table 3.4: Results with regular and random distributions

It can be perceived from the results that tensile properties vary less, specially in the longitudinal direction, which was expected since we are using only one element in length. However, the different transverse section arrangements cause the shear properties to have higher deviations, specially those associated with the first and second directions x and y.

[2]It is important to refer that, as previously mentioned, the longitudinal fibre direction corresponds to the third direction z

For low values of fibre volume fraction, the differences are mainly due to the varying fibre spacing. When a regular distribution is applied, the space between neighbouring fibres is almost uniform, but for random fibre packings there may be neighbouring fibres very close and others further away. The discrepancy in these neighbouring distances is accentuated for low fibre volume fractions as it was also seen previously in Section 2.4.2.

For the standard values of fibre volume fraction ($V_f = 60\%$), the transverse shear moduli computed show the highest deviations, with regular fibre arrangements giving an overall underestimation of the elastic properties of the material when compared to random packings. This is why it is important to model composite behaviour using transverse randomness of reinforcement, which portrays better the reality of fibre distributions in a composite material. Between different fibre random arrangements, the results were also compared and it could be seen that a maximum increase of about 10% in fibre properties could be reached with different fibre distributions. Thus, it should be possible to arrange the fibres so that the material equivalent properties are optimized (e.g. maximized), as was already studied by Leal [44].

The values for the number of nodes and elements were shown in order to study the response of the FE mesh generator Gmsh to the complex geometries obtained with random distributions. It can be seen that, specially when the fibre volume fraction is high, the number of nodes and elements created increases if fibres are randomly arranged in the RVE transverse section. This is explained by some meshing errors that may occur when the fibres are to close between them or to the RVE boundaries. These errors consist in the generation of smaller elements than those in general, which does not happen when the fibres are uniformly spaced as in a regular distribution. Figure 3.10 illustrates one of the random distributions obtained along with the regular distribution analysed for $V_f = 60\%$, and the meshing errors that might take place are shown in Figure 3.11.

Other errors might take place in the PREMAT meshing module MESH3D due to the distance between nodes in the same face when periodic boundary conditions are assigned. The assignment of PBC results from a search for the nodes in opposite sides of the RVE that are equivalent and provide the geometric continuity. The search for this nodes is made taking into account a small deviation in the coordinates of the nodes, with a thin search area around the point of interest. If two points are too close, in this area there might be more than one point, which will cause the wrong assignment of PBC. This can be fought by increasing the radius dimensions of the fibres in powers of 10, since it does not change anything in the PREMAT computations.

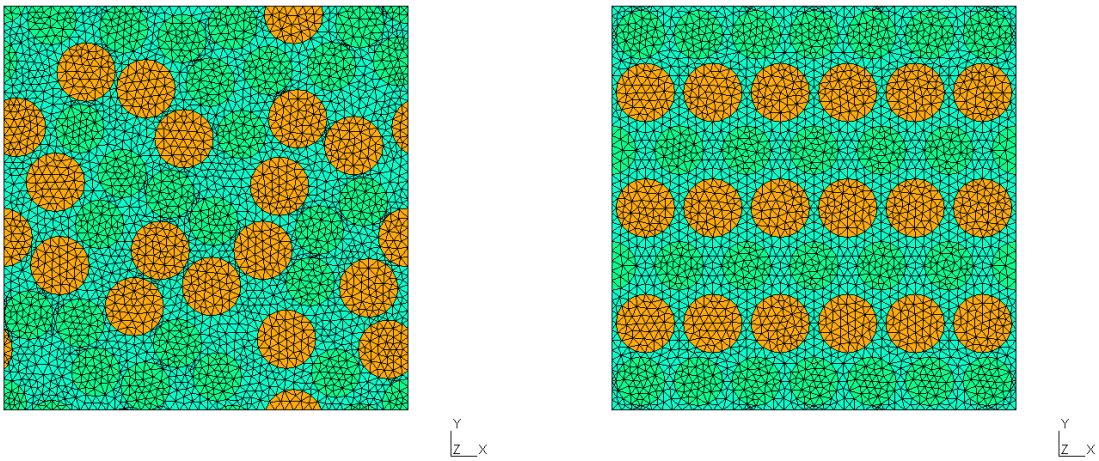

(a) Random distribution

(b) Regular distribution

Figure 3.10: Analysed meshes for $V_f = 60\%$.

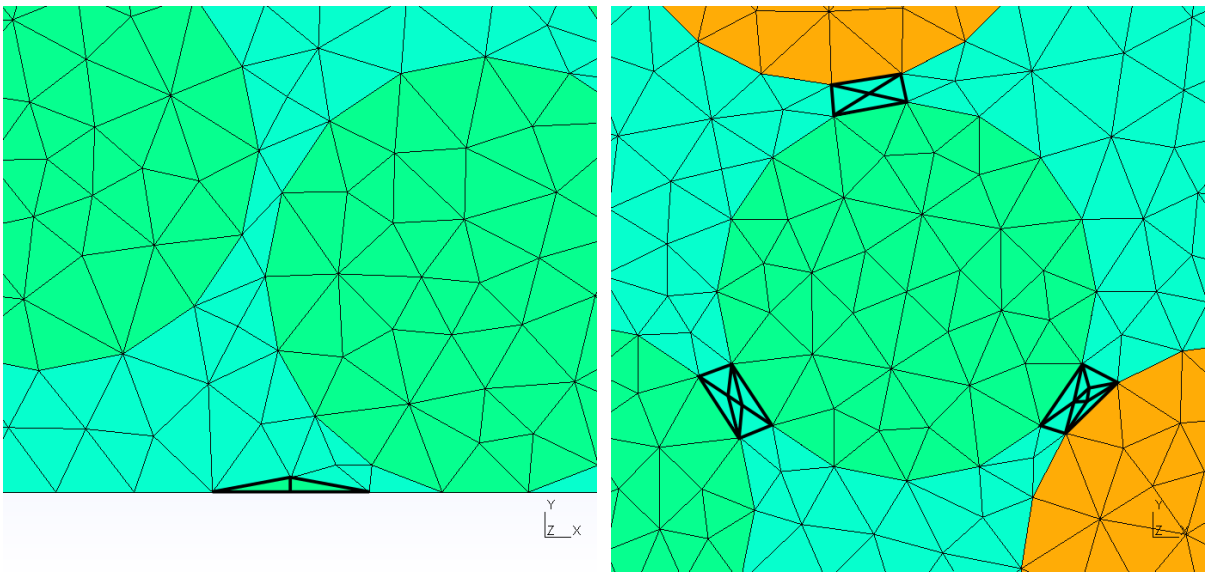

(a) Fibres close to the boundaries

(b) Fibres close between each other

Figure 3.11: Meshing error situations.

Chapter 4

Damage Model

In this chapter the model developed to induce damage on the generated RVE will be presented. The model is a three-dimensional finite element model which makes use of POSTMAT [25] program to apply strains and compute the stresses in the microstructure, as a sequence of the computational models developed in the previous chapters.

4.1 Problem Description

The problem consists in applying uniaxial traction by imposing deformation on the generated 3D RVE in order to plot the stress-strain curve and study the damage on the composite material by sequential fibre breaking. The primary goal is to model the failure mechanisms of UD composites and to understand how hybridization can change the mechanical behaviour of composite materials, mostly regarding pseudo-ductility. Further objectives include comparisons with simpler models, more specifically with the spring element model (SEM) used by Tavares et al. [23].

To compute the strains, displacements and stresses on the RVE, POSTMAT makes use of PREMAT results file `bkaiso.txt` containing the homogenized compliance matrix of the material and the deformation modes utilized in the homogenization computations. The deformation modes `X11, X22, X33, X13, X23, X12` contain the nodal displacements resulting from loading the RVE in each one of these six directions. These local microdeformations will be used in POSTMAT as input, defining the behaviour of the microstructure in each direction. Along with the compliance matrix, by applying strain or stress in one or more chosen directions, POSTMAT is able to compute the nodal strains and stresses in all directions, and with the nodal information, it also computes the information for each element of the mesh.

The deformation will be imposed by applying strain in the longitudinal direction of the fibres and the stresses will be computed from this coupling between PREMAT and POSTMAT in all shear and tensile directions. However, in this work the only stress that will be taken into account is the one corresponding to the inflicted strain direction, in our case the third direction z, which will be assumed as the principal

stress. POSTMAT results for the stresses in each element of the microstructure are outputted in the file `seqso.txt`. The stress in a single fibre is calculated from a weighted sum of the element stresses corresponding to that fibre. The assignment of the elements for each fibre must take into account the periodic continuity imposed to the RVE, not forgetting about the fibres that are split between opposite sides of the RVE or in its corners. The stress in a fibre f is thus obtained from the following equation:

$$\sigma^f = \frac{\sum V_e^f \sigma_e^f}{\sum V_e^f} \tag{4.1}$$

where V_e^f and σ_e^f correspond respectively to the volume and stress for an element of the fibre f. The volume of the element is calculated from the coordinates of the nodes that constitute it (in our case the four nodes of the tetrahedron). The use of this equation is based on the assumption that, as we are applying strain only in the longitudinal direction of the fibres, the deviations in the element stresses of the same fibre will not be significant.

Once the stress in the fibre is calculated, we define the failure criterion for a fibre f:

$$\sigma^f > \sigma_T^f \tag{4.2}$$

meaning that if the stress computed for a given fibre, σ^f, surpasses the tensile strength assigned for that fibre, σ_T^f, the fibre will be considered broken. The matrix is assumed to have no failure associated throughout the process, meaning that the failure of the composite is controlled solely by fibre breaks.

As the finite element mesh generated considers just one element in length, the failure of a fibre is considered catastrophic for that fibre, i.e. there is no concern about the definition of ineffective length. The assumption made is that the fibre will continue there, but loose its rigidity. This situation is modelled by reducing significantly the Young's modulus of the broken fibre for the subsequent computations.

4.2 Numerical Model

The numerical implementation was made using MATLAB® script `complete_analysis`, and it is illustrated in Figure 4.1. All scripts present in the previous chapters are used along with the input variables and parameters studied, including the radius of the fibres, the RVE size parameter δ, the required volume fraction V_f and the element size parameter `lc`.

The model starts by running `randgenGA` to generate the RVE cross-section. From the random fibre distribution obtained, the mesh is created and then extruded in Gmsh, to form the 3D finite element grid. The material properties are assigned to fibres and matrix, namely the Young's moduli E_f and E_m and the Poisson's ratios ν_f and ν_m, and then each fibre is given a different tensile strength based on the Weibull distribution [6] for fibre bundles.

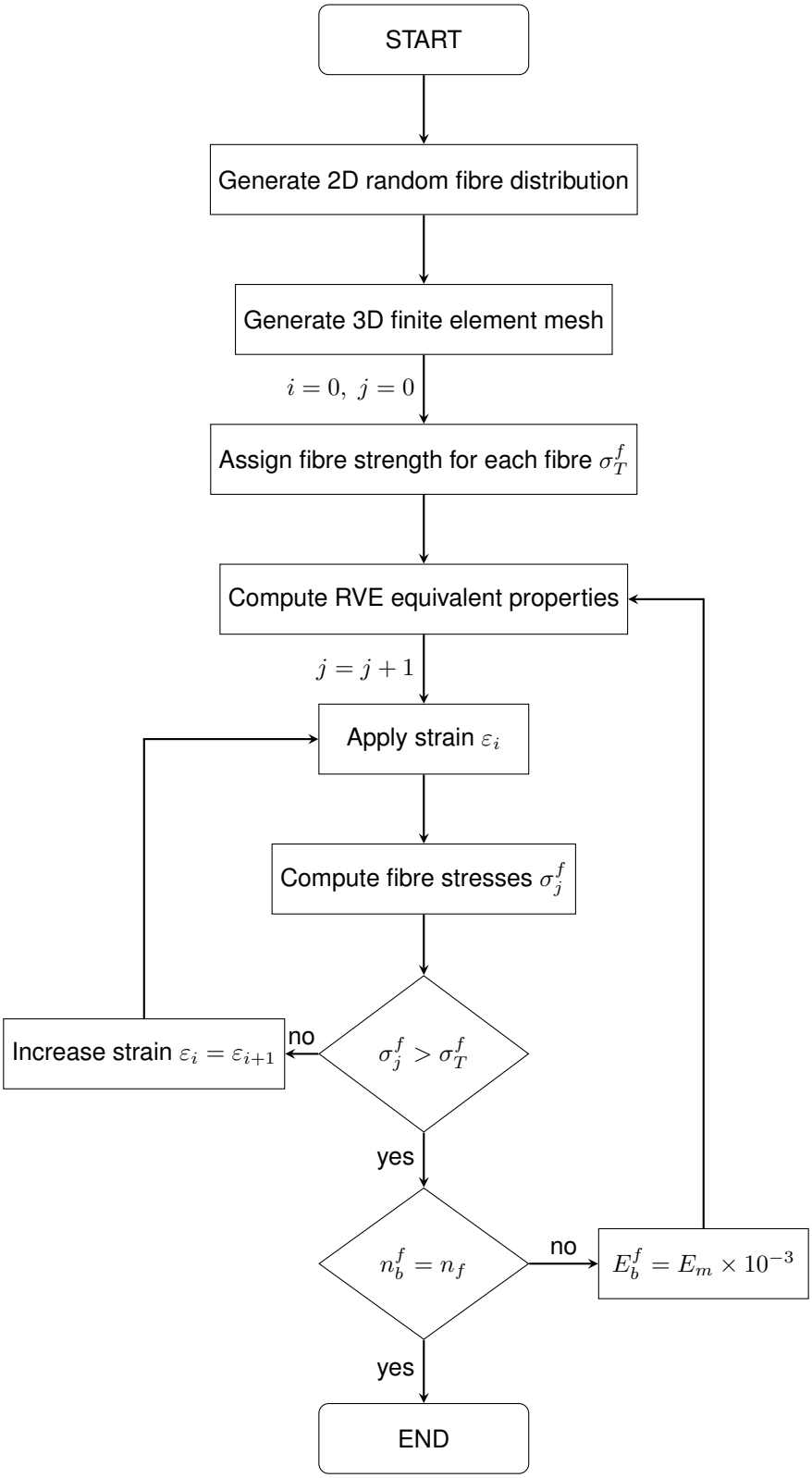

Figure 4.1: Flowchart for the damage model.

The Weibull probability distribution is given by:

$$P(\sigma) = 1 - exp\left[-\frac{L}{L_0}\left(\frac{\sigma}{\sigma_0}\right)^m\right] \tag{4.3}$$

where P is the failure probability at the applied stress σ, L is the characteristic gauge length, L_0 is the reference gauge length, σ_0 the scale parameter and m the shape parameter or Weibull modulus [6].

The assignment of the fibre strength for each fibre is done by randomly generating a number $X \in [0, 1]$ that will represent the probability P in Equation (4.3), and then the tensile strength for each fibre is calculated from:

$$\sigma_T^f = \sigma_0\left[-\frac{L_0}{L}ln(1-X)\right]^{\frac{1}{m}} \tag{4.4}$$

Once the mesh is generated and the fibre tensile strength is calculated, the mesh is exported to PREMAT as explained in Section 3.2.2 and the homogenized properties for the RVE are computed, as well as the deformation modes that will be used in POSTMAT.

In the first analysis a small strain ε_0 is applied so that no fibre breaks occur. As long as there are no fibre breaks, we have a linear relation between stress and strain in the composite. Figure 4.2 illustrates the predicted behaviour of this model. Note that σ_0 now is not the same of that in Equations (4.3) and (4.4), it corresponds to the stress obtained when a strain ε_0 is applied.

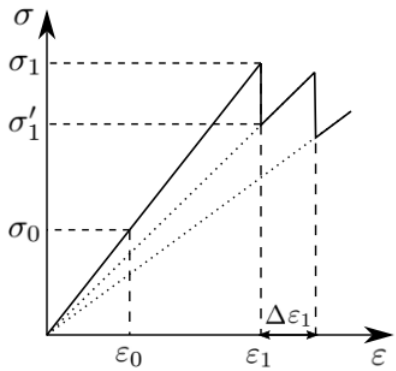

Figure 4.2: Stress-strain behaviour for the damage model.

As the strain applied is equally distributed along the transverse section, from the POSTMAT result for the stresses on the fibres in this first computation σ_0^f, we assume that there is also a linear proportion between the applied strain and the fibre stresses given by σ_0^f/ε_0. This means that to reach the failure strength σ_T^f for the first fibre we need to take into account the stress in each fibre and with this linear relation find the first strain ε_1 required for a fibre to break:

$$\varepsilon_1 = min\left(\frac{\sigma_T^f}{\sigma_0^f/\varepsilon_0}\right) \tag{4.5}$$

The resulting stress σ_1^f must meet the failure criterion (4.2) so that the first fibre breaks. However, underestimations due to numerical losses might occur in the strain ε_1 calculated, such that no fibre breaks occur. The solution is to add a very small increment so that the strain applied causes the fibre failure as expected. Another reason for this underestimations might be the fact that we are only accounting for the stresses in the z direction. The total stress in a fibre is divided through the six directions from the Poisson's effect, and although the shear stresses are insignificant, the tensile stresses in the transverse directions x and y also affect the composite behaviour.

If the failure criterion is met, the number of broken fibres n_f^b is updated and the Young's modulus of the broken fibre is reduced to $E_f^b = E_m \times 10^{-3}$. To permit this changes in the broken fibres properties, the fibres are considered each one an independent material having its own properties. Since this fibre properties were modified, the model will compute the homogenized material constants again in PREMAT and with the same strain compute the stresses for the new homogenized material. This will cause a new value for the linear relation between stress and strain as illustrated by the dotted lines in Figure 4.2. In order to achieve a more detailed curve, the next increment of strain will be calculated with the purpose of ensuring that the fibres fail one-by-one:

$$\Delta\varepsilon_i = min\left(\frac{\sigma_T^f - \sigma_i^{f\prime}}{E_f}\right) \tag{4.6}$$

where i corresponds to the number of broken fibres at some stage of the numerical implementation, i.e $i = 1, ..., n_f$ where n_f is the total number of fibres. The $\sigma_i^{f\prime}$ represents the new stress computed with the same strain applied as given in Figure 4.2. Therefore, Equation (4.6) means that the next fibre that will break is the one where the most recent computed stress is closer to its tensile strength. The strain in the next computation will be given by:

$$\varepsilon_{i+1} = \varepsilon_i + \Delta\varepsilon_i \tag{4.7}$$

and applied to the new homogenized material.

All strains and average stresses ε_i, σ_i and σ_i' computed for the entire RVE (fibres and matrix) are saved and the process ends with the stress-strain curve response for the composite material plotted when all fibres are broken, i.e. when $n_f^b = n_f$.

Chapter 5

Results

The damage model will be implemented in microstructures representing carbon fibre reinforced composite materials. The results provided consist in the analysis of the behaviour of two non-hybrid composites and the hybridization considered the two different fibres used. The choice of the materials and parameters of hybridization are based on previous studies developed by Tavares et al.[21, 23]. The influence of considering different RVE geometries and different tensile strength distributions in the damage model is analysed due to the randomness of the geometry generator and in the implementation of the Weibull distribution for the fibre bundle.

5.1 Mechanical properties

As stated, two different carbon fibres were chosen with the ultimate goal of creating an hybrid composite capable of representing a pseudo-ductile behaviour. The materials must have different failure strains so that the HE fibres only begin to fail when most of the LE fibres have already failed. The fibre materials that will be utilized in the computations are the AS4 carbon and the M50S carbon, which Weibull parameters and elastic properties are represented in Table 5.1.

Material	Reference	σ_0 (MPa)	L_0 (mm)	m	E_f (GPa)	R (μm)
AS4 carbon	Curtin 1998 [45]	4275	12.7	10.7	234	3.5
M50S carbon	Tanaka 2014 [46]	4600	10	9	480	2.65

Table 5.1: Mechanical properties for carbon fibres.

For the matrix the assigned properties are those of an epoxy resin with $E_m = 4.6$ GPa and $\nu_m = 0.4$. The Poisson's ratio for the carbon fibres selected is a typical value of $\nu_f = 0.35$. These parameters will not implicate much influence on the results for the tensile failure of UD composites, thus their choice does not need to be precise.

In sequence of the previous chapters, the considered RVEs have side dimensions $a = 15 \times R$ with 1 unit of length in the z direction and the mesh element size parameter `lc`=$a/40$. The values for the gauge length L are neglected by implying $L = L_0$ in the Weibull formula (4.3).

5.2 Influence of fibre distribution

For the same Weibull distribution of tensile strength, five different RVE geometries with random fibre packing were analysed for a composite material containing 60% of AS4 carbon fibres. The geometries obtained are shown in Figure 5.1.

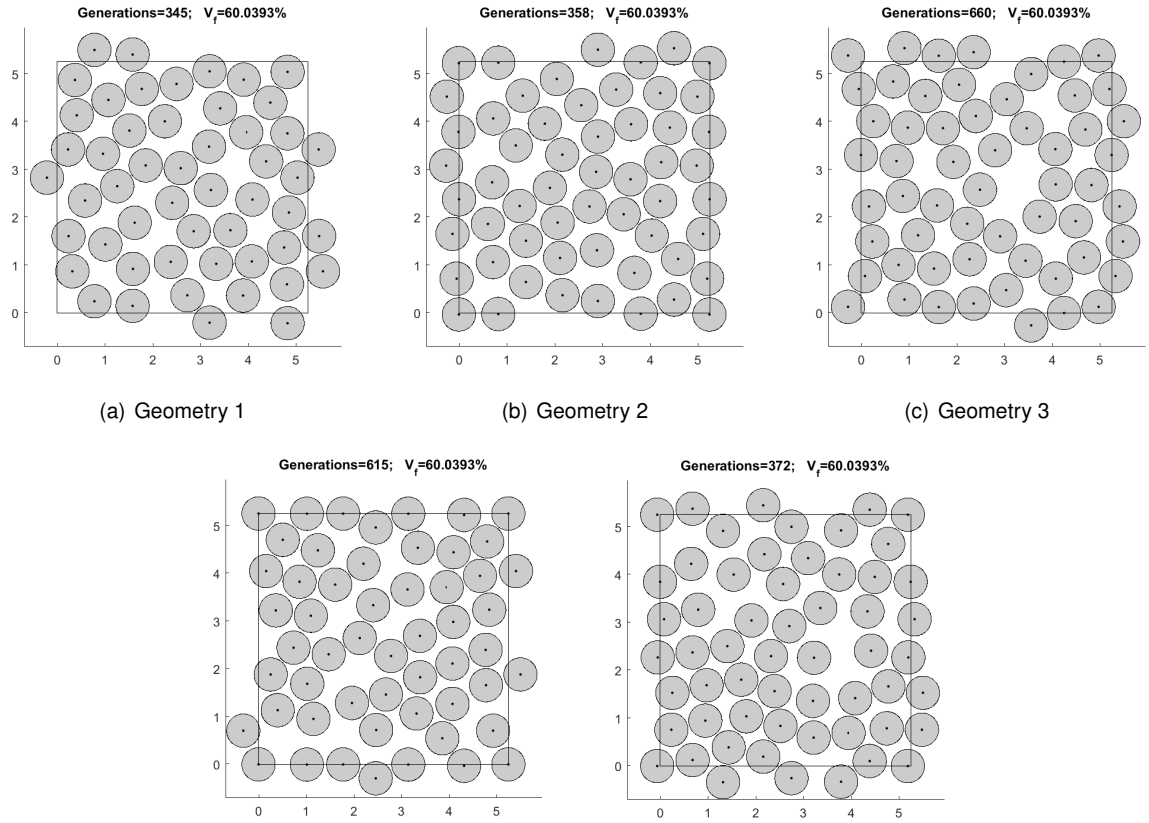

(a) Geometry 1 (b) Geometry 2 (c) Geometry 3

(d) Geometry 4 (e) Geometry 5

Figure 5.1: Analysed RVE geometries.

The resulting data in Table 5.2 specifies the strain necessary for the first fibre to fail ε_1 and the respective value of the average stress computed in the microstructure σ_1, the maximum average stress σ_{max} reached by the composite material and the correspondent strain ε and also the last strain applied for each simulation, which will be referred as the ultimate failure strain but in reality is only the strain at which the last fibre failure occurs on the RVE. Figure 5.2 illustrates the stress-strain curves for the five simulations with a different color for each of the geometries analysed.

Simulation	ε_1 (%)	σ_1 (MPa)	σ_{max} (MPa)	ε @ σ_{max} (%)	ε_f (%)
1	1.38	2114	2114	1.38	2.09
2	1.37	2098	2098	1.37	2.09
3	1.37	2097	2097	1.37	2.09
4	1.38	2110	2110	1.38	2.09
5	1.38	2115	2115	1.38	2.09
Average	1.38	2107	2107	1.38	2.09
STDV	0.01	8.70	8.70	0.01	0.00

Table 5.2: Initial failure strain and stress, maximum stress and ultimate failure strain for different fibre arrangements.

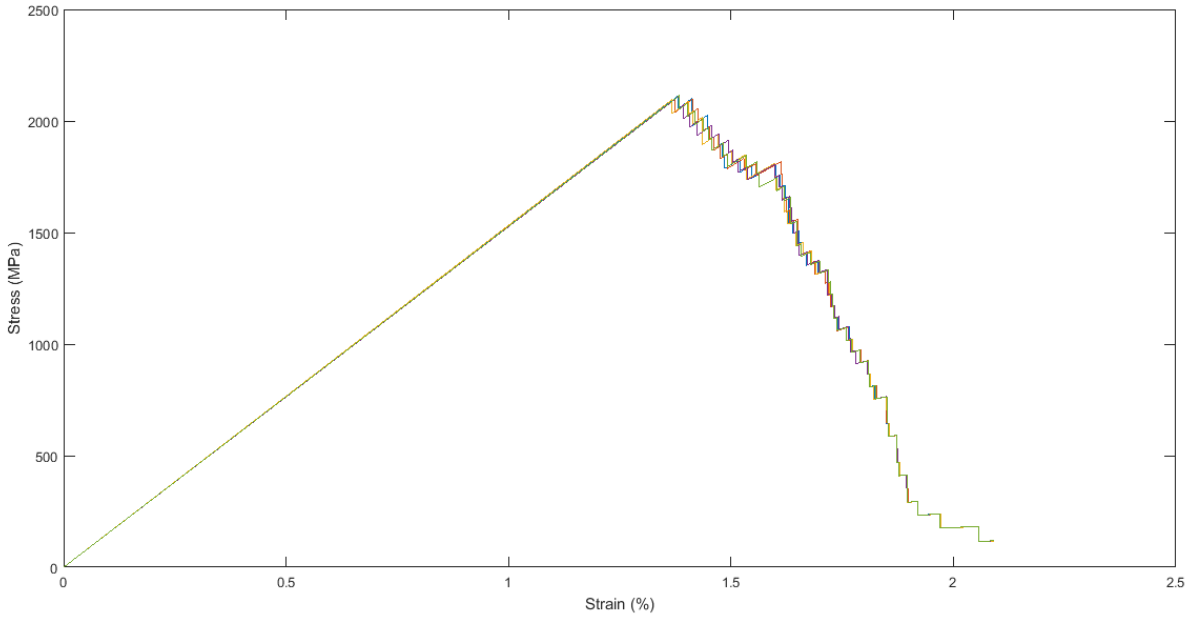

Figure 5.2: Stress-strain behaviour of AS4 composite for different fibre arrangements.

It is clear that varying the fibre distribution on the RVE does not lead to changes in the mechanical response of the UD composite to tensile loads. As we are applying strains only taking into account the longitudinal response, the damage model implies dependencies almost only in the longitudinal tensile properties. These properties were seen the ones that suffered less deviations for different random distributions in Chapter 3, and thus this behaviour should be expected. Notice how the standard deviations tabled are almost insignificant and the first fibre to break is always coincident with the maximum stress, proving the catastrophic failure of non-hybrid composites. Moreover, from the stress-strain diagram we can see how the behaviours are similar leading to matching curves. However, it is important to mention that small changes might occur in the fibre breaking sequence due to clustering, since the space between fibres is variable.

5.3 Influence of tensile strength distribution

In this section, for the same RVE geometry, five different runs were made with different Weibull distributions for the tensile strength of AS4 carbon fibre reinforced composite and M50S carbon fibre composite, with 60% fibre volume fraction. The FE mesh for each of the fibre materials is displayed in Figure 5.3. The performance of the different runs is shown in Tables 5.3 and 5.4 and by the stress-strain behaviour in Figures 5.4 and 5.5.

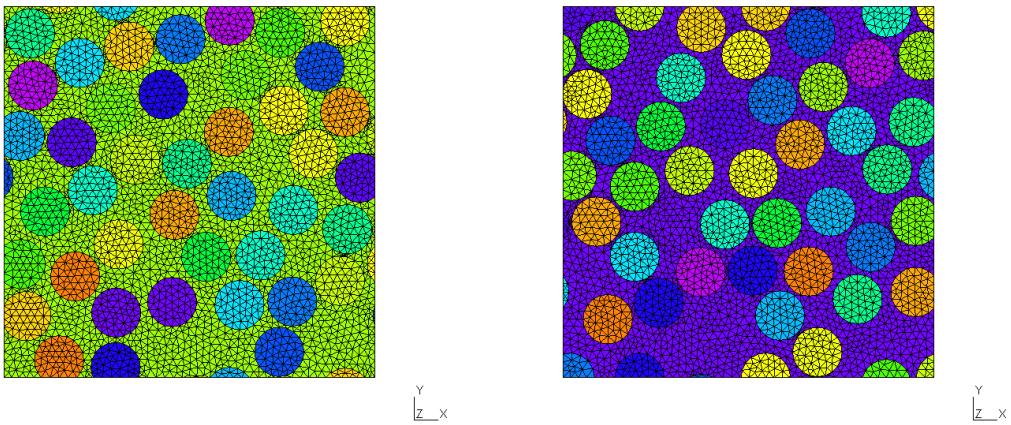

(a) AS4 carbon reinforced composite (b) M50S carbon reinforced composite

Figure 5.3: RVE FE meshes generated.

Simulation	ε_1 (%)	σ_1 (MPa)	σ_{max} (MPa)	ε @ σ_{max} (%)	ε_f (%)
1	1.38	2114	2114	1.38	2.09
2	1.13	1721	2014	1.36	2.07
3	1.25	1908	1938	1.56	2.04
4	1.07	1642	1952	1.39	2.08
5	1.26	1923	1923	1.26	2.05
Average	1.22	1861.60	1988.20	1.39	2.07
STDV	0.11	165.90	70.10	0.10	0.02

Table 5.3: Initial failure strain and stress, maximum stress and ultimate failure strain for different AS4 fibre strength distributions.

Looking either to the standard deviations tabled either to the stress-strain behaviour of both composites we can perceive that varying the fibre strength distribution has much more influence than varying the geometry of the analysed microstructure. It can be seen that the values for the initial failure strain have the most significant variation for both fibre types, as well as the corresponding composite strength at that level, with standard deviations of 165.90 and 208.25 MPa for this later value for the AS4 and M50S composites, respectively. However, using only distributions depending on Weibull's equation does not yet significantly change the composite response. Applying modified versions of the Weibull distribution as the ones developed by Curtin [8] and Peterlik and Loidl [7] would lead to much more different behaviours.

Simulation	ε_1 (%)	σ_1 (MPa)	σ_{max} (MPa)	ε @ σ_{max} (%)	ε_f (%)
1	0.59	1750	2102	0.78	1.14
2	0.68	2023	2023	0.68	1.16
3	0.57	1705	1975	0.70	1.08
4	0.53	1586	1868	0.72	1.06
5	0.69	2064	2148	0.76	1.12
Average	0.61	1826	2023	0.73	1.11
STDV	0.07	208.25	109.77	0.04	0.04

Table 5.4: Initial failure strain and stress, maximum stress and ultimate failure strain for different M50S fibre strength distributions.

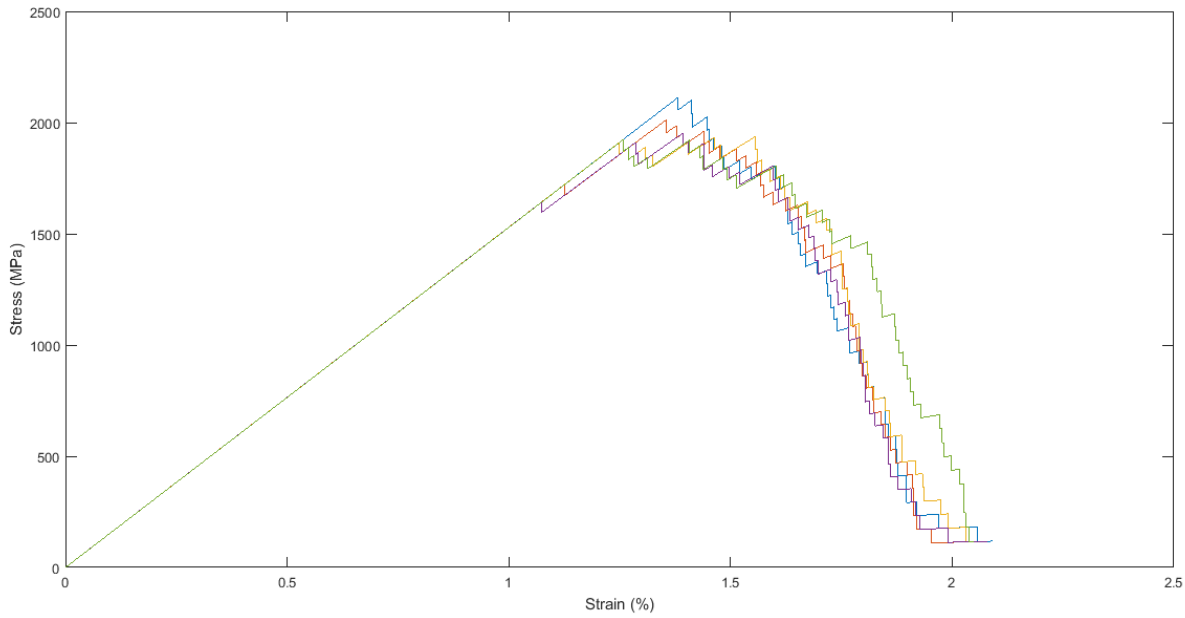

Figure 5.4: Stress-strain behaviour of AS4 composite for different tensile strength distributions.

The first fibre break does not always lead to the decrease of the composite average stress as diverse tensile strength distributions may assign very low values to the weakest fibres, compared to the average of the tensile strength distribution. The discrepancies between fibre tensile strengths difficult the prediction of stress redistribution after a fibre breaks, since it is not clear the existence of clusters of broken fibres nor is it clear to assume the fibres break in a random way as per order of the tensile strength.

From the results it is clear which fibre type will be the LE fibre and which will be the HE fibre for hybridization, as the failure strains for the M50S fibre reinforced composite have much lower values than those obtained with AS4 reinforcement.

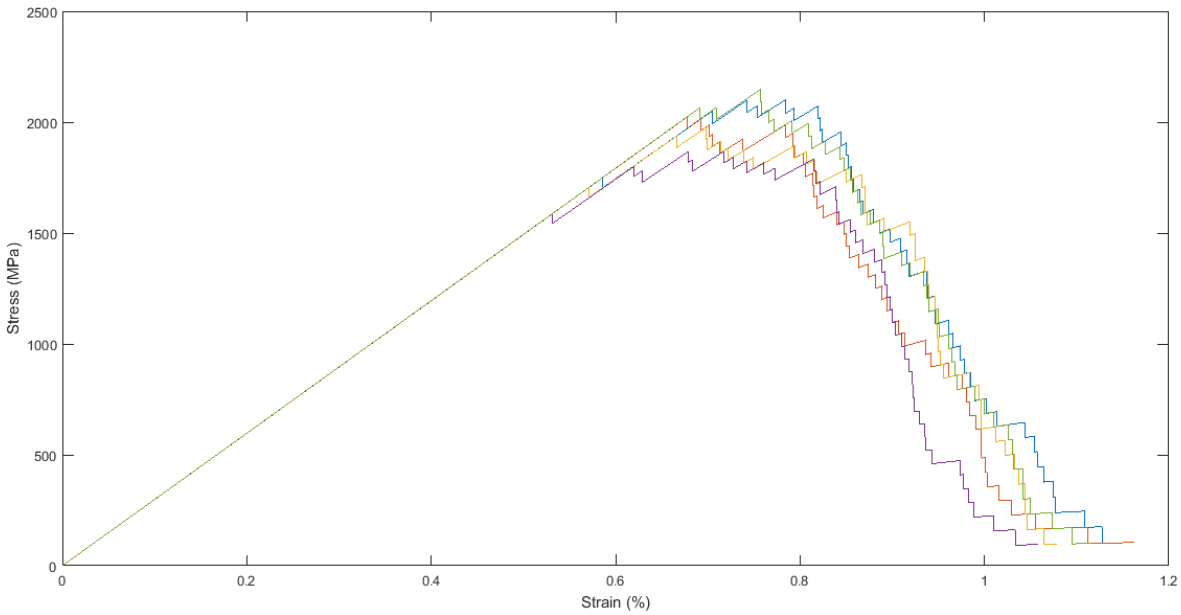

Figure 5.5: Stress-strain behaviour of M50S composite for different tensile strength distributions.

5.4 Carbon-carbon hybridization

Based on the prediction of the hybrid dry tow model in [21] and of the spring element model in [23], the hybrid volume fraction of HE fibres AS4 used is 80%, with 20% of LE fibre M50S content. The geometry and mesh obtained for the hybrid configuration with an overall fibre volume fraction of 60% are illustrated in Figure 5.6.

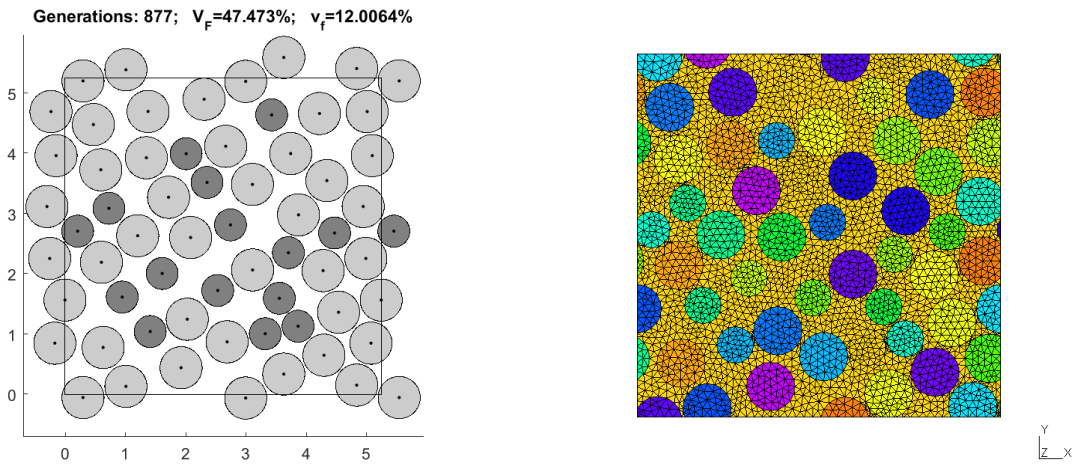

(a) RVE geometry generated

(b) RVE FE mesh generated

Figure 5.6: Hybrid configuration.

We study again how different fibre strength distributions might change the composite behaviour, with the results tabled in Table 5.5 and plotted in Figure 5.7.

Simulation	ε_1 (%)	σ_1 (MPa)	σ_{max} (MPa)	ε @ σ_{max} (%)	ε_f (%)
1	0.57	1031	1435	1.41	2.11
2	0.70	1257	1697	1.55	2.03
3	0.80	1435	1597	1.42	2.05
4	0.40	719	1439	1.23	2.08
5	0.53	952	1652	1.46	2.02
Average	0.60	1079	1564	1.41	2.06
STDV	0.15	276.75	121.23	0.12	0.04

Table 5.5: Initial failure strain and stress, maximum stress and ultimate failure strain for different AS4-M50S hybrid fibre strength distributions.

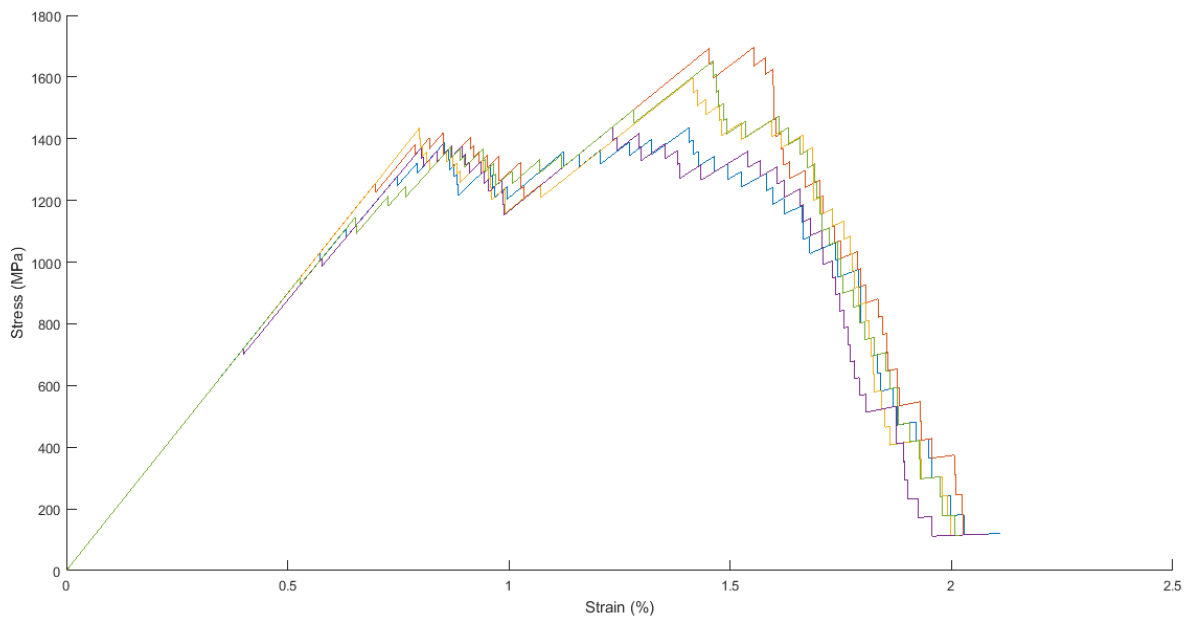

Figure 5.7: Stress-strain behaviour of hybrid AS4-M50S composite for different tensile strength distributions.

It is well noticeable how both fibre types complement each other. From Table 5.5 we can observe that the strain at maximum stress is always fairly higher than the first fibre failure strain, and specifically for the third simulation, it is curious how this difference does not translate in a big deviation between the maximum stress achieved and the one computed for the first fibre break.

It is again important to observe how the initial failure strain varies for the diverse distributions of strength. From the stress-strain behaviour in Figure 5.7, it can be seen that the tensile strength distribution affects a lot the quest for pseudo-ductility. While the curve in red demonstrates a standard hybrid composite behaviour, the blue curve represents a closer pseudo-ductile response.

For a better comprehension of the hybrid effect, the stress-strain curves are plotted simultaneously in Figure 5.8 for an all AS4 fibre and an all M50S reinforced non-hybrid composite, along with the configuration studied for the carbon-carbon hybridization. The results from Tavares et al. [23] are also shown for the same hybridization for comparison.

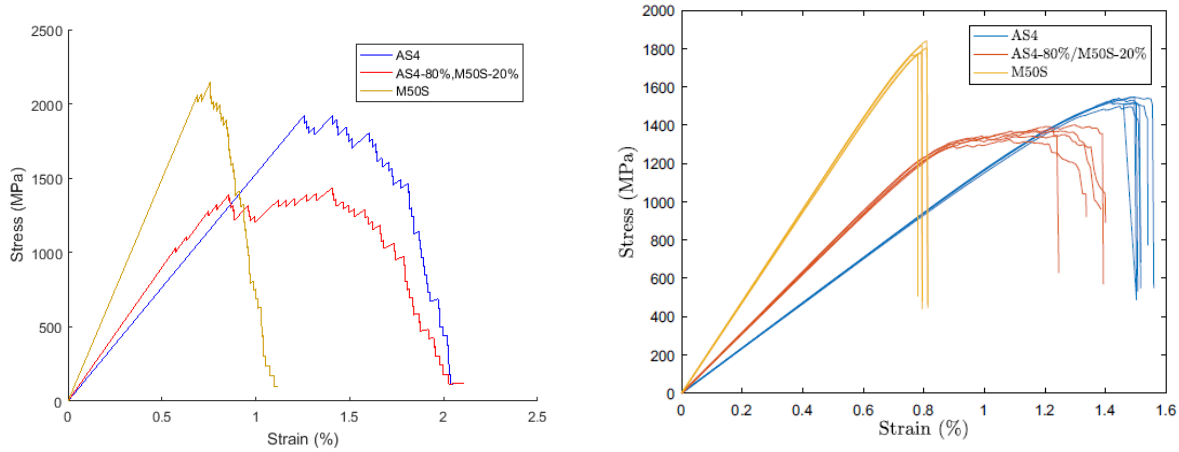

(a) Results obtained using the developed model

(b) Results obtained by Tavares et al. [23] using SEM

Figure 5.8: Stress-strain behaviour comparison for AS4 (blue) and M50S (yellow) non-hybrid composites and AS4-M50S (red) hybrid composite.

Regarding the continuous finite element model developed in this work, from Figure 5.8(a), along with the values obtained in Table 5.5, it is seen how the initial failure strain corresponds to the initial failure strain of the LE fibre and the ultimate failure strain is similar to that of the HE fibre. The predominance of the HE fibre content is clear by the slope of the stress-strain line before the first peak corresponding to the initial fibre break. From there, although not being completely constant, the average stress computed for the composite material microstructure does not face significantly high deviations as the strain increases, having a tendency for the achievement of pseudo-ductility. However, the hybridization causes a clear decrease in the composite strength when compared to both of the non-hybrid behaviours.

Looking to the results for the same hybridization conducted by Tavares et al. [23] with the spring element model we can see that the behaviour is similar but there are still differences mostly because this model has the capacity of using many more fibres due to its computational simplicity. This can create a stress-strain line where the peaks that we see in Figure 5.8(a) are less noticeable, since they are very close to each others due to the high number of fibres. Another difference has to do with the ultimate failure situation. We can see that the behaviour at ultimate failure in Figure 5.8(b) illustrates the sudden way the composite fails with a vertical line. This happens because the damage model developed by Tavares et al. [23], although also breaking the fibres one-by-one, considers the damage of the matrix as well, with the failure of the spring elements connecting the fibres.

5.5 Stress distribution

An analysis of the stress distributions obtained in POSTMAT at important stages of the simulation is made for a better understanding of the mechanics of fibre failure. The stress distributions that cause the first and last fibre breaks for the non-hybrid composite RVEs studied are shown in Figures 5.9 and 5.10, respectively for the AS4 and the M50S reinforced structures.

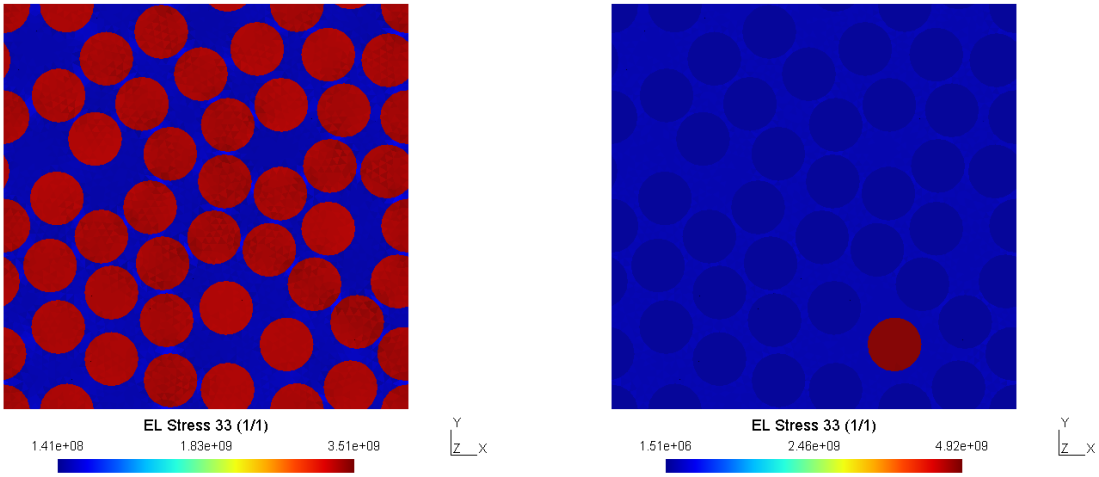

(a) Initial failure (b) Final failure

Figure 5.9: Element stress distributions for AS4 reinforced RVE.

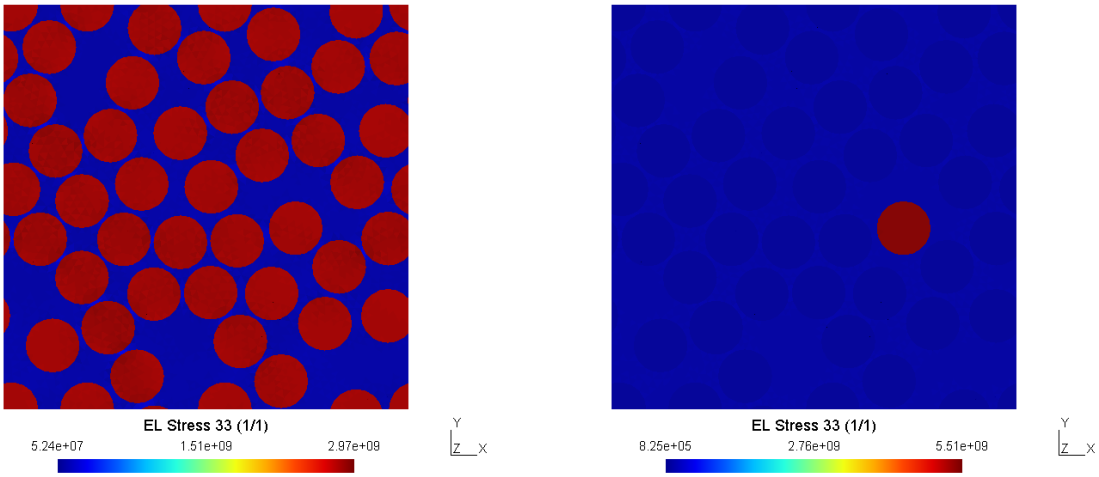

(a) Initial failure (b) Final failure

Figure 5.10: Element stress distributions for M50S reinforced RVE.

From the figures correspondent to the initial failure we can see how all fibres carry nearly the same stress, and how the stress distribution is uniform within a single fibre, thus validating the calculation of the stress by the weighted average of the element stresses. This implies that the first fibre to break will be almost certainly the one with the lowest tensile strength. Also, the last fibre to break is probably the one with the highest strength. From the results illustrated we see the maximum values of stress in the longitudinal direction, from where we can take the range of fibre strength. For the AS4 fibres the range goes from 3.51 GPa to 4.92 GPa and for the MS0S fibres the fibre strength has values between 2.97 GPa and 5.51 GPa. Notice that the M50S range is larger due to its Weibull distribution parameters. However, the fibres do not always break in the ascending order of tensile strength. Cluster phenomena might occur when there are neighbour fibres that break causing a stress redistribution to the intact fibres that are closer. From comparing the ascending order of tensile strength and the fibre breaking order the simulations confirmed this theory, making it clear the matrix affects the stress redistribution. Without the matrix all fibres would always have exactly the same values of stress, breaking only respecting the tensile strength order.

For the hybrid configuration we look at the stress distributions again for the initial and final fibre failure, but now we will also analyse the stress distribution that cause the last LE fibre to break and the first HE fibre to break. The resulting element stresses for this four situations are presented in Figure 5.11.

The first thing noticed is that the low number of M50S fibres caused a narrower range of tensile strength when compared to the range for the non-hybrid M50S reinforced composite, with the value for the first of this type of fibres failure of 3.5 GPa higher than the 2.97 GPa previously obtained and the value for the last M50S carbon fibre failure of 5.05 GPa lower than the 5.51 GPa achieved above. However, since the AS4 carbon content is high in this hybridization as the HE fibre, the values for the tensile strength seem to have the same range. From Figure 5.11(a) it is clear how the LE fibres withstand most of the stress in the microstructure.

We can see how all LE fibres broke before the HE fibres start to break, which is not the perfect way for a pseudo-ductile response. For this kind of response the HE fibres should start to fail when most, but not all, LE fibres already failed. The strain applied for the stress distribution in Figure 5.11(b) is $\varepsilon = 0.0103$ and for Figure 5.11(c) is $\varepsilon = 0.145$, which is a high deviation, since if we want a pseudo-ductile behaviour, even if all LE fibres break first, these strains should be as close as possible. Furthermore, we can see that when the last LE fibre break the stress in the HE fibres is 2.53 GPa, which is yet far from the stress it takes for the first HE fibre to fail of 3.61 GPa.

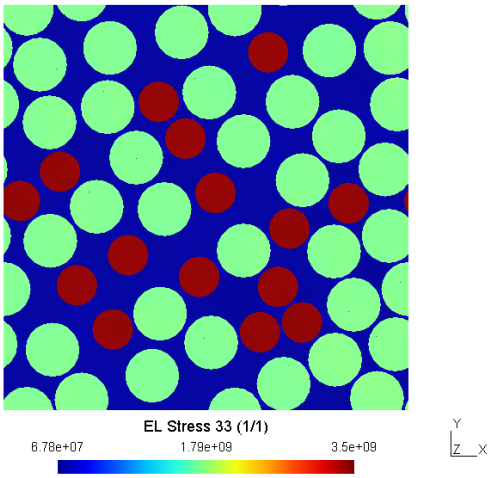

(a) Initial failure

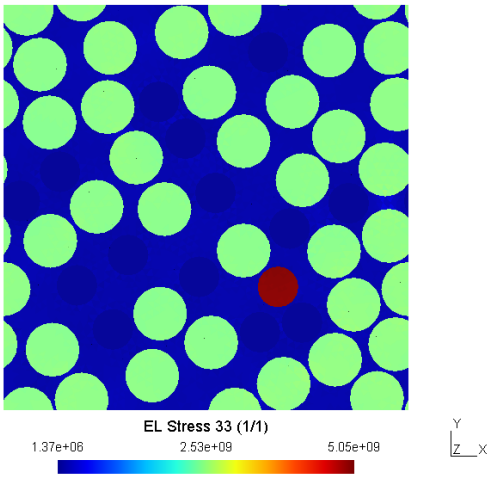

(b) Last LE fibre break

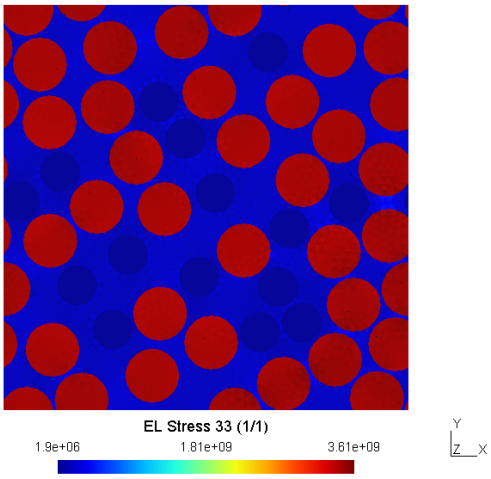

(c) First HE fibre break

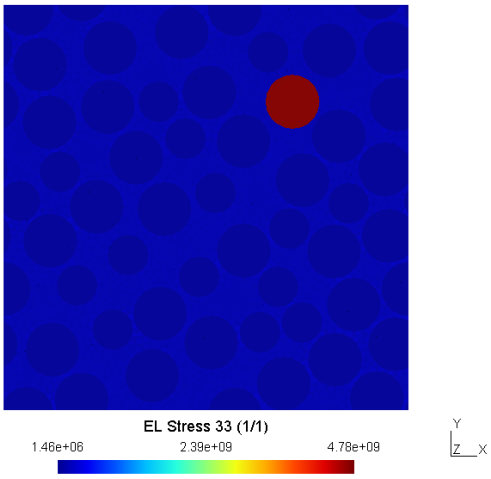

(d) Final failure

Figure 5.11: Element stress distributions for AS4-M50S hybrid reinforced RVE.

Chapter 6

Conclusions

This chapter summarizes the main conclusions of the thesis, reporting its primary developments and results achieved. Future work to improve knowledge in the field of hybrid composites and micromechanical modelling is also proposed.

6.1 Achievements

This work first achievement was the successful development of a new methodology to generate transverse randomness of reinforcement. The optimization approach using the genetic algorithm proved to be efficient for high fibre volume fractions, although more time spending compared to the high performance algorithm developed by Melro [28]. For fibre hybrid configurations with two different radius the algorithm had a good performance as well, and the fact that it can be easily adapted to allow more fibre radius might become useful. However, the Cuckoo Search [31] algorithm implementation was not that successful, as enormous amounts of time were spent to reach fibre volume fractions of 60%. The big limitation of `randgenGA` is the inability to create fibre arrangements for high values of the RVE size parameter δ.

In Chapter 3 a path was created in order to compute the equivalent properties for the RVE geometry generated. The 3D CAD engine and the mesh generator of Gmsh proved to be compatible to the PREMAT program used for obtaining the homogenized elastic constants. The parametric studies showed that the problem of not being able to produce big sized RVEs with larger number of fibres changes the calculated constants, although the deviations are not significant. However, the main achievement in this chapter was the confirmation of the underestimation of the Young and shear moduli for regular fibre packings when compared to random packings [17], which was specially spotted for the shear moduli with high fibre volume fraction. This is one more step to the statement that it is essential for a better micromechanical analysis of composite materials to consider random fibre arrangements which portray a closer geometry to the reality of fibrous materials.

The damage model implemented used POSTMAT capabilities of stress computation to predict the com-

posite behaviour when tensile loads are applied in the microstructure through the imposition of average strain in the longitudinal direction. The big difference between this and the SEM model [23] is the continuity provided by the 3D finite element mesh with the fibres embedded in the matrix rather than having only one element connecting it to a neighbouring fibre. This provides a more complete model with higher complexity and demand of computational effort.

The results of Section 5.2 proved that the RVE geometry does not influence the response of the analysed composite material to longitudinal tension. This goes in accordance with the results in Chapter 3 that showed the property with the less deviation is the one representing the longitudinal tensile properties, since we are only taking into account the stresses in this direction, where the strain is applied.

The varying tensile strength distributions, however, has more influence on the stress-strain behaviour of the composite materials. From Section 5.3 results one can observe that different tensile strengths affect the most the initial failure strain and corresponding value for the average stress in the analysed microstructures. Still, the value for the ultimate failure strain was very close in all runs.

In the hybridization conducted with the two different fibre types AS4 and M50S carbon fibres the choice of the Weibull distribution to assign the tensile strength to the fibres leads to an higher variation of the results. It was seen that the hybrid composite has an initial failure strain equal to the LE fibre and an ultimate failure strain equal to the HE fibre, as well as the strain obtained for the maximum stress withstood. However, the values for the stress at the first fibre break and the maximum stress decrease significantly for the hybrid configuration. The pseudo-ductility is hardly achieved and not for all fibre strength distributions. Nevertheless, it is noticeable that there is a tendency for a more ductile behaviour, which could be better reached if more fibres were taken into consideration. The fact that there are only 15 LE fibres does not allow the best estimations for the overall hybrid composite behaviour, but the estimation achieved closely relates to the ones obtained by Tavares et al. [23] for the SEM model and the micromechanical model in [21] for the same hybridization.

6.2 Future Work

The model developed in this thesis despite of predicting reasonably well the composite behaviour has some flaws that can be sustained in future works.

For start, the random generator developed can be fine tuned to withstand a larger number of design variables in the genetic algorithm optimization. This way a larger RVE could be created and more fibres will fit, which would create a more detailed stress-strain curve. However, the simplicity of the random fibre generator and the easy application of more different fibre radius could serve to study how using hybridization with more than two different fibre materials would affect the mechanical behaviour of the composite. It is clear that with more than two fibre materials the achievement of pseudo-ductility could

become much easier.

Another interesting study that could have use with this model is the effect of fibre dispersion in hybrid composites. Swolfs et al. [15] made a research explaining how the fibre dispersion can lead to better performances of the hybrid composite and Conde et al. [47] provided an optimization method for the achievement of pseudo-ductility by controlling the dispersion degree using SEM. These models were implemented with regular distributions of fibres, thus it would be interesting to use random fibre arrangements and study this dispersion degree which creates a pseudo-ductile behaviour.

The model can also be of use for predicting the stress redistribution around a broken fibre, as it computes the stresses for each fibre and compares them to their assigned tensile strength. This way, the process of sequential fibre breaking could be studied with the objective of finding if the failure of the composite is caused by clustering or in random manner.

Overall, the pseudo-ductile behaviour has only been achieved for low fractions of LE fibres and therefore their mechanical properties are reduced. New strategies need to be developed to achieve this behaviour in higher LE fibre fractions.

Bibliography

[1] K. K. Chawla. *Fibrous Materials*. Cambridge University Press, 1998. ISBN:0521570794.

[2] Safran. The aerospace materials of the future. Safran Group website, 03/2018. URL `https://www.safran-group.com/media/aerospace-materials-future-20170925`.

[3] W. Wang, Y. Dai, C. Zhang, X. Gao, and M. Zhao. Micromechanical modeling of fiber-reinforced composites with statistically equivalent random fiber distribution. *MDPI: Journal of Materials Science*, 2016. doi:10.3390/ma9080624.

[4] R. Hill. Elastic properties of reinforced solids: Some theoretical principles. *Journal of the Mechanics and Physics of Solids*, 11(5):357—372, 1963.

[5] S. Pimenta, A. Mersch, and M. Alves. Predicting damage accumulation and fatigue life of UD composites under longitudinal tension. *IOP Conference Series: Materials Science and Engineering*, 2018. doi:10.1088/1757-899X/388/1/012007.

[6] W. Weibull. A statistical distribution function of wide applicability. *Journal of Applied Mechanics - Transactions of the ASME*, 58(7):1001—-1010, 1951.

[7] H. Peterlik and D. Loidl. Bimodal strength distributions and flaw populations of ceramics and fibres. *Engineering Fracture Mechanics*, 68(3):253—-261, 2001.

[8] W. A. Curtin. Tensile strength of fiber-reinforced composites: Iii. beyond the traditional weibull model for fiber strengths. *Journal of Composite Materials*, 34:1301–1332, 2000.

[9] Y. Swolfs, I. Verpoest, and L. Gorbatikh. Issues in strength models for unidirectional fibre-reinforced composites related to weibull distributions, fibre packings and boundary effects. *Composites Science and Technology*, 114:42 – 49, 2015. ISSN 0266-3538. doi: https://doi.org/10.1016/j.compscitech.2015.04.002.

[10] A. Hansen, P. C. Hemmer, and S. Pradhan. *The Fibre Bundle Model*. Wiley, 2015.

[11] Y. Swolfs, I. Verpoest1, and L. Gorbatikh1. Tensile failure of hybrid composites: measuring, predicting and understanding. *IOP Conference Series: Materials Science and Engineering*, 2016. doi:10.1088/1757-899X/139/1/012008.

[12] B. W. Rosen. Tensile failure of fibrous composites. *AIAA Journal*, 2:1985–1991, 1964.

[13] C. Zweben. Tensile strength of hybrid composites. *Journal of Materials Science*, 12(7):1325 – 1337, 1977.

[14] Y. Swolfs, L. Gorbatikh, and I. Verpoest. Fibre hybridisation in polymer composites: A review. *Composites Part A: Applied Science and Manufacturing*, 67:181 – 200, 2014. ISSN 1359-835X. doi: https://doi.org/10.1016/j.compositesa.2014.08.027.

[15] Y. Swolfs, R. M. McMeeking, I. Verpoest, and L. Gorbatikh. The effect of fibre dispersion on initial failure strain and cluster development in unidirectional carbon/glass hybrid composites. *Composites Part A: Applied Science and Manufacturing*, 69:279 – 287, 2015. ISSN 1359-835X. doi: https://doi.org/10.1016/j.compositesa.2014.12.001.

[16] Y. Swolfs, L. Gorbatikh, V. Romanov, S. Orlova, S. Lomov, and I. Verpoest. Stress concentrations in an impregnated fibre bundle with random fibre packing. *Composites Science and Technology*, 74:113 – 120, 2013. ISSN 0266-3538. doi: https://doi.org/10.1016/j.compscitech.2012.10.013.

[17] A. Wongsto and S. Li. Micromechanical finite element analysis of unidirectional fibre-reinforced composites with fibres distributed at random over the transverse cross-section. *Composites: Part A*, 36(9):1246 – 1266, 2005.

[18] D. Trias, J. Costa, J. Mayugo, and J. Hurtado. Random models versus periodic models for fibre reinforced composites. *Computational Materials Science*, 38(2):316 – 324, 2006. ISSN 0927-0256. doi: https://doi.org/10.1016/j.commatsci.2006.03.005.

[19] Y. Swolfs. *Hybridisation of Self-reinforced Composites: Modelling and Verifyinga Novel Hybrid Concept*. PhD thesis, KU Leuven, 2015.

[20] A. Turon, J. Costa, P. Maimí, D. Trias, and J. Mayugo. A progressive damage model for unidirectional fibre-reinforced composites based on fibre fragmentation. part i: Formulation. *Composites Science and Technology*, 65(13):2039 – 2048, 2005. ISSN 0266-3538. doi: https://doi.org/10.1016/j.compscitech.2005.04.012.

[21] R. P. Tavares. Mechanics of hybrid polymer composites. Master's thesis, Faculty of Engineering of the University of Porto, 2015.

[22] F. Conde, P. Coelho, R. Tavares, P. Camanho, J. Guedes, and H. Rodrigues. Optimization of hybrid polymer composites under uniaxial traction. *Engineering Computations*, 35(2):904–931, 2018. doi: 10.1108/EC-11-2017-0427.

[23] R. P. Tavares, F. Otero, A. Turon, and P. P. Camanho. Effective simulation of the mechanics of longitudinal tensile failure of unidirectional polymer composites. *International Journal of Fracture*, 208(1):269–285, Dec 2017. ISSN 1573-2673. doi: 10.1007/s10704-017-0252-9. URL `https://doi.org/10.1007/s10704-017-0252-9`.

[24] T. Okabe, H. Sekine, K. Ishii, M. Nishikawa, and N. Takeda. Numerical method for failure simulation of unidirectional fiber-reinforced composites with spring element model. *Composites Science and*

Technology, 65(6):921 – 933, 2005. ISSN 0266-3538. doi: https://doi.org/10.1016/j.compscitech.2004.10.030.

[25] J. M. Guedes and N. Kikuchi. Preprocessing and postprocessing for materials based on the homogenization method with adaptive finite element methods. *Computer Methods in Applied Mechanics and Engineering*, 83:143–198, 1990.

[26] V. Buryachenko, N. Pagano, R. Kim, and J. Spowart. Quantitative description and numerical simulation of random microstructures of composites and their effective elastic moduli. *International Journal of Solids and Structures*, 40(1):47 – 72, 2003.

[27] S. Yang, A. Tewari, and A. M. Gokhale. Modeling of non-uniform spatial arrangement of fibers in a ceramic matrix composite. *Acta Materialia*, 45(7):3059 – 3069, 1997.

[28] A. R. Melro. *Analytical and Numerical Modelling of Damage and Fracture of Advanced Composites*. PhD thesis, Faculdade de Engenharia da Universidade do Porto, 2011.

[29] D. E. Goldberg. *Genetic Algorithms in Search, Optimization and Machine Learning*. Addison Wesley, 1989. ISBN:0-201-15767-5.

[30] J. S. Arora. *Introduction to Optimum Design*. Elsevier, 4th edition, 2017. ISBN: 978-0-12-800806-5.

[31] X.-S. Yang and S. Deb. Engineering optimisation by cuckoo search. *Int. J. Mathematical Modelling and Numerical Optimisation*, 1(4):330 – 343, 2010.

[32] C. Brown, L. S. Liebovitch, and R. Glendon. Lévy flights in dobe juhoansi foraging patterns. *Human Ecol.*, 35:129 – 138, 2007.

[33] Mathworks. `ga` - find minimum of function using genetic algorithm. R2018b documentation, 05/2018. URL `https://www.mathworks.com/help/gads/ga.html`.

[34] Mathworks. Genetic algorithm options. R2018b documentation, 05/2018. URL `https://www.mathworks.com/help/gads/genetic-algorithm-options.html`.

[35] Mathworks. Vary mutation and crossover. R2018b documentation, 05/2018. URL `https://www.mathworks.com/help/gads/vary-mutation-and-crossover.html`.

[36] M. Angelova and T. Pencheva. Tuning genetic algorithm parameters to improve convergence time. *International Journal of Chemical Engineering*, 2011. doi:10.1155/2011/646917.

[37] G. W. Milton. *The Theory of Composites*. Cambridge University Press, 2002. ISBN:0-521-78125-6.

[38] P. Ciarlet and M. Rouseau. On homogenization problems. In O. Oleinik, editor, *Trends and Applications of Pure Mathematics to Mechanics*. Springer, 1984.

[39] O. Oleinik, A. Shamaev, and G. Yosifian. *Mathematical Problems in Elasticity and Homogenization*, volume 26 of *Studies in Mathematics and Its Applications*. North-Holland, 1991. ISBN:0-444-88441-6.

[40] N. Charalambakis. Homogenization and micromechanics. *Bulletin of the Greek Mathematical Society*, 57:115 – 123, 2010.

[41] T. I. Zohdi and P. Wriggers. *An Introduction to Computational Micromechanics*. Springer, 2004.

[42] C. Geuzaine and J.-F. Remacle. Gmsh: a three-dimensional finite element mesh generator with built-in pre- and post-processing facilities. *International Journal for Numerical Methods in Engineering*, 79(11):1309 – 1331, 2009.

[43] Gmsh. Gmsh reference manual, 05/2018. URL `http://gmsh.info/doc/texinfo/gmsh.html`.

[44] F. Leal. Computational characterization and optimization of hybrid composites reinforced with two types of fiber of different materials. Master's thesis, Instituto Superior Técnico, 2016.

[45] W. A. Curtin and N. Takeda. Tensile strength of fiber-reinforced composites: Ii. application to polymer matrix composites. *Journal of Composite Materials*, 32(22):2060–2081, 1998.

[46] J. Watanabe, F. Tanaka, H. Okuda, and T. Okabe. Tensile strength distribution of carbon fibers at short gauge lengths. *Advanced Composite Materials*, 23(5-6):535–550, 2014. doi: https://doi.org/10.1080/09243046.2014.915120.

[47] F. Conde, P. Coelho, R. Tavares, P. Camanho, J. Guedes, and H. Rodrigues. Optimization of unidirectional hybrid polymer composites using a spring element model. 6th Engineering Optimization Conference, 2018.

Appendix A

Flowcharts for RAND_uSTRU_GEN

The descriptive flowcharts of the algorithm RAND_uSTRU_GEN developed by Melro [28], including the three steps describing the hard-core model and the two heuristics, are shown in Figures A.1-A.4. For further knowledge of each step procedures and identification of the nomenclature see [28].

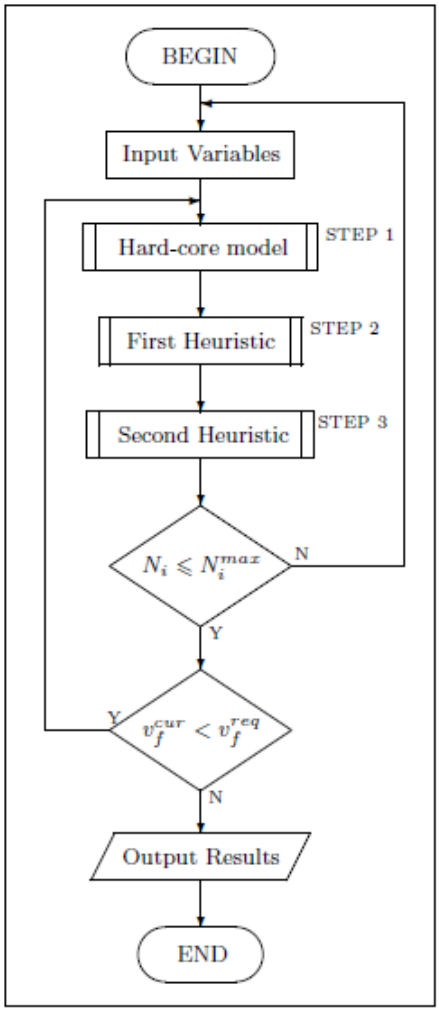

Figure A.1: Flowchart of algorithm RAND_uSTRU_GEN [28].

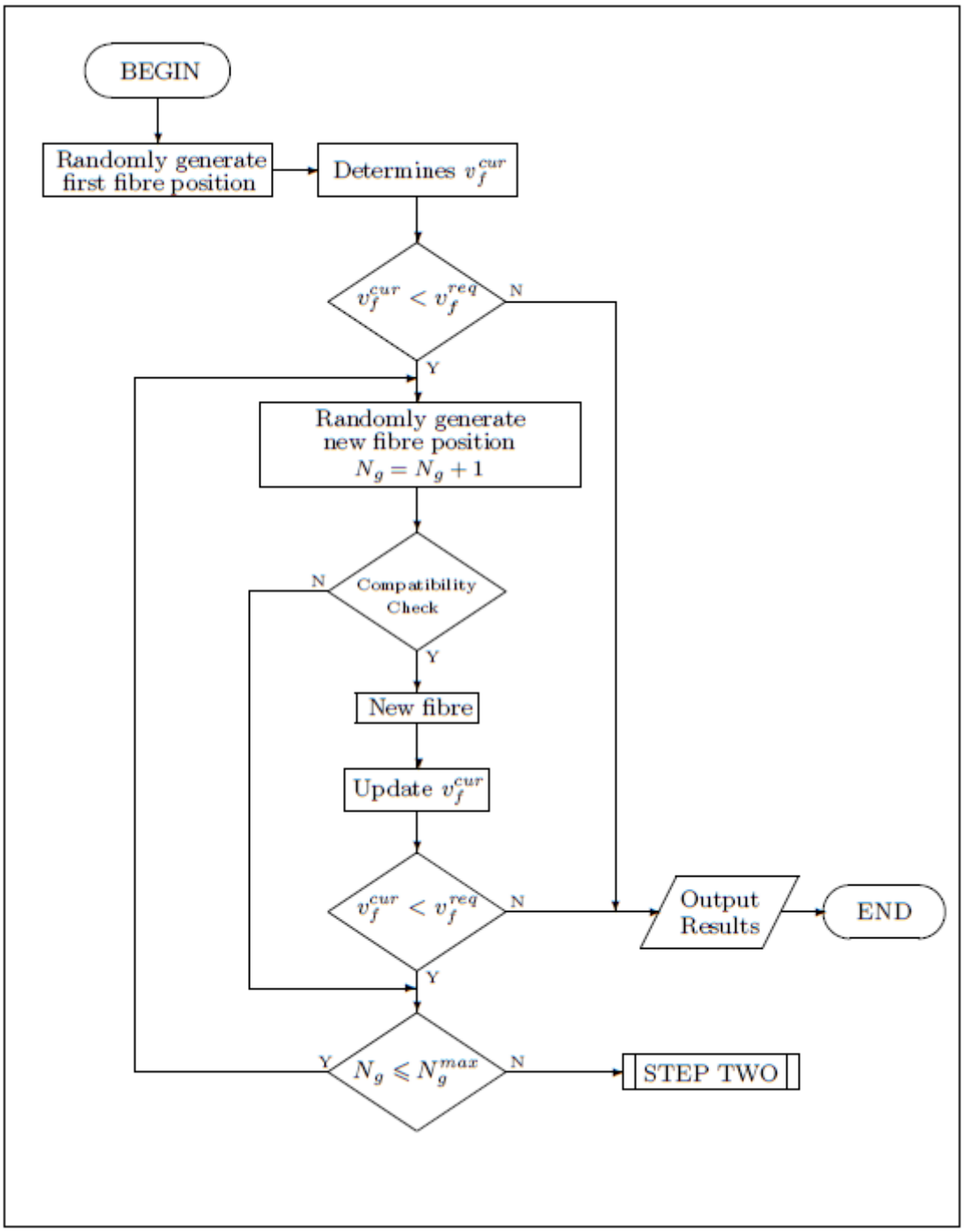

Figure A.2: Flowchart of STEP ONE [28].

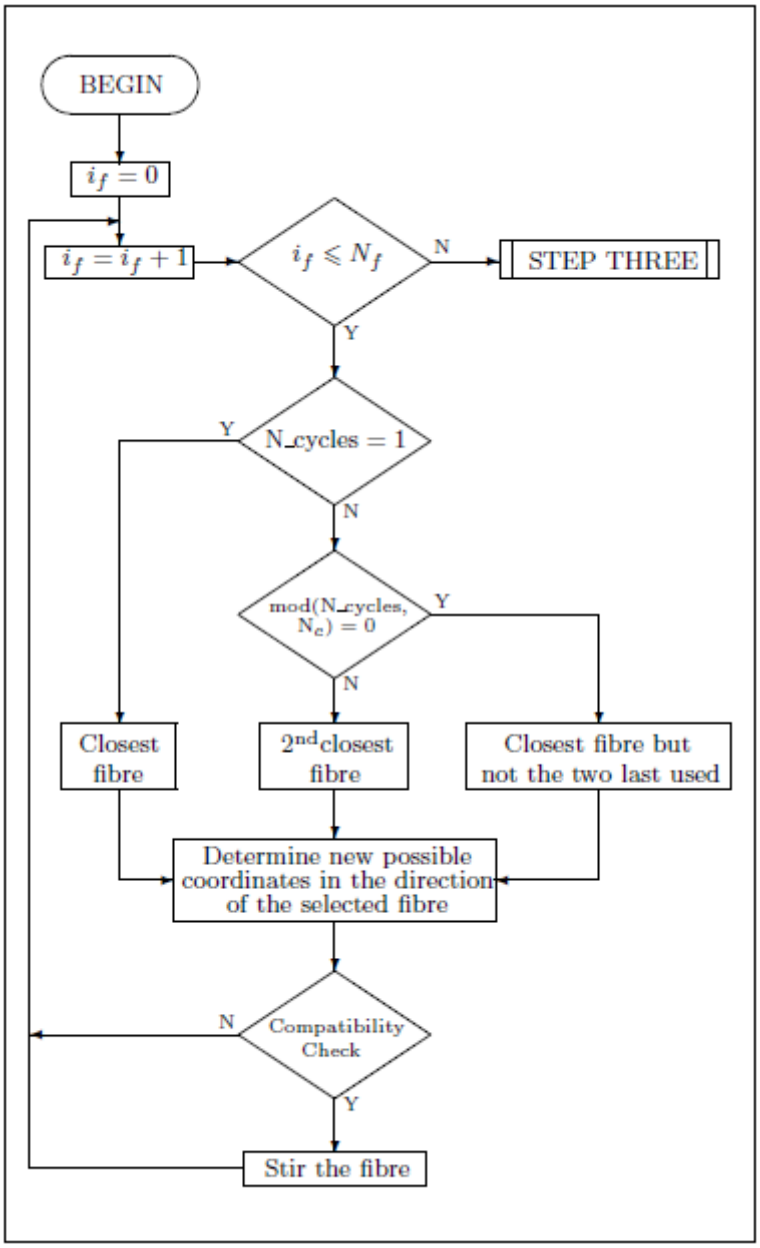

Figure A.3: Flowchart of STEP TWO [28].

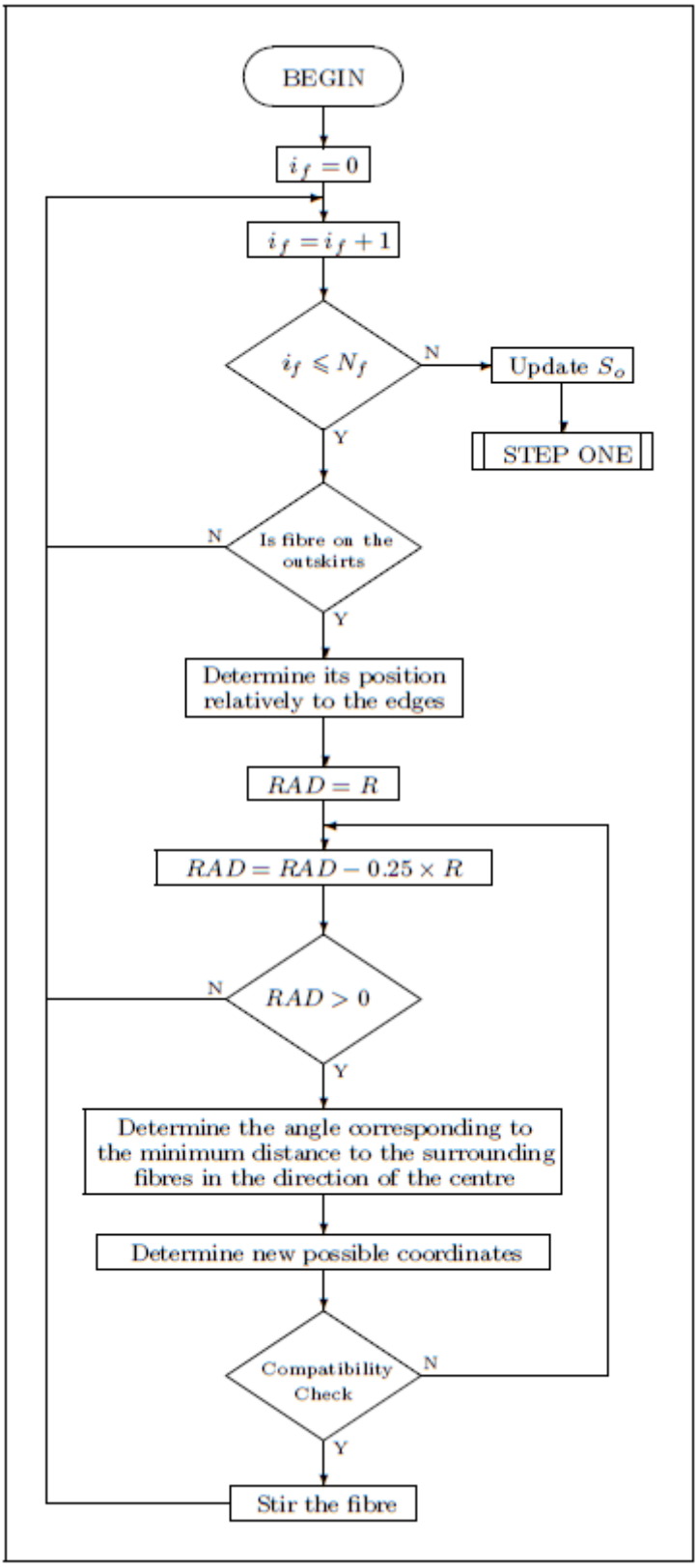

Figure A.4: Flowchart of STEP THREE [28].